Power uprates
and plant life extension

CASL-U-2014-0032-000

Consortium for Advanced Simulation of LWRs

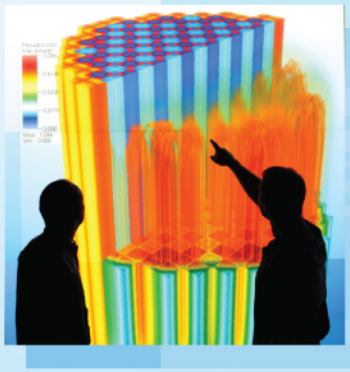

Engineering design
and analysis

Assessment of Multi-Scale Thermal-Hydraulic Codes and Models for DNB Challenge Problem Applications L3.AMA.CP.P8.01

Science-enabling
high performance
computing

Yixing Sung, Jin Yan, Liping Cao,
Vefa N. Kucukboyaci, Emre Tatli
Westinghouse Electric Company LLC

Mark A. Christon, Jozsef Bakosi
Los Alamos National Laboratories

Robert K. Salko
Oak Ridge National Laboratories

Hongbin Zhang
Idaho National Laboratory

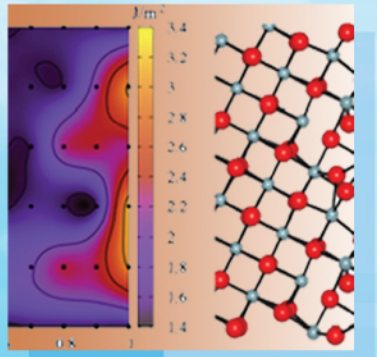

Fundamental science

Plant operational data

March 31, 2014

U.S. DEPARTMENT OF ENERGY | Nuclear Energy

REVISION LOG

Revision	Date	Affected Pages	Revision Description
0	03/31/2014	All	Initial Issuance

Document pages that are:

Export Controlled _____N/A _____

IP/Proprietary/NDA Controlled _____N/A _____

Sensitive Controlled _____N/A _____

Requested Distribution:

To:

Zeses E. Karoutas, AMA FA Lead
Jeff Banta, CASL Program Manager

Copy:

CASL SLT Team
CASL ELT Team
Jin Yan, AMA, WEC
Robert K. Salko, PHI, ORNL
Leslie E. Nipper, ORNL
Hongbin Zhang, AMA, INL

EXECUTIVE SUMMARY

The objectives of this milestone work are to assess the improved capabilities of the multi-scale thermal-hydraulic (T/H) codes and models developed by the Consortium for Advanced Simulation of Light Water Reactors (CASL) for Departure from Nucleate Boiling (DNB) Challenge Problem (CP), in accordance with the DNB CP implementation plan. The multi-scale models can range from fine mesh Computational Fluid Dynamics (CFD) simulation of flow field surrounding a fuel rod to a full core modeling of a Pressurized Water Reactor (PWR). The assessments are performed based on the CASL subchannel code COBRA-TF (CTF) and the CFD code Hydra-TH.

Significant improvements have been achieved on the CASL multi-scale T/H code and modeling capabilities based on the CTF subchannel code and the Hydra-TH CFD code in the past year for DNB CP applications. The improvements are reflected in the new transient modeling for the Reactivity Insertion Accident (RIA) DNB predictions and full assembly modeling using the CTF code and its processor, as well as the rod bundle modeling for single-phase flow and heat transfer simulations using the Hydra-TH code, the pre-processor for mesh generation and the post-processor for data visualization. The following code capabilities have been demonstrated in the assessment:

- The modeling and simulation of the TK experiments demonstrated that CTF is able to simulate a fast transient with a large power pulse.

- The CTF preprocessor was found to be very helpful in greatly reducing the model creation effort and minimizing human error for large model setup such as a subchannel model for the entire 17x17 fuel assembly. A reasonably fast CTF execution time can be achieved with the Krylov solver with the large model.

- The modeling and simulation of the 3x3 subchannel geometry under single phase flow conditions have been successfully completed using the Hydra-TH CFD code including mesh generation and result visualization. The Hydra-TH results indicate the similar capabilities of the subchannel single phase fluid solutions as compared to the STAR-CCM+ results.

The code and model assessments also indicated additional improvements needed for the planned DNB CP applications. Recommendations on code-specific improvements are listed in Section 6 of the report.

CONTENTS

FIGURES

TABLES

ACRONYMS

AMA	Advanced Modeling Applications
CASL	Consortium for Advanced Simulation of Light Water Reactors
CFD	computational fluid dynamics
CHF	critical heat flux
COBRA-TF	Coolant Boiling in Rod Arrays – Two Fluids
CP	challenge problem
CPU	central processing unit
CTF	COBRA-TF subchannel code
DNB	departure from nucleate boiling
DNBR	departure from nucleate boiling ratio
DOE	U.S. Department of Energy
FA	focus area
FWHM	full width at half maximum
GWD/MTU	Giga-Watt-Day per Metric Ton of Uranium
HFP	hot full power
IAF	inverted annular flow
IFM	Intermediate Flow Mixer (grid spacer)
JAERI	Japan Atomic Energy Research Institute
LANL	Los Alamos National Laboratory
M&S	modeling and simulation
MDNBR	Minimum DNBR
MV	mixing vane (grid spacer)
NDA	non-disclosure agreement
NSRR	Nuclear Safety Research Reactor (Japan)
OD	outside diameter
OECD	Organization for Economic Co-operation and Development
ORNL	Oak Ridge National Laboratory
PCMI	pellet-to-clad mechanical interaction
PHI	Physics Integration Focus Area
PSU	Pennsylvania State University
RIA	Reactivity Insertion Accident
PWR	pressurized water reactor
RAM	random access memory
SPL	single phase liquid
STAR-CCM+	Simulation of Turbulence in Arbitrary Regions-Computational Continuum Mechanics
SUBC	subcooled boiling
T-H (or T/H)	thermal-hydraulics
THM	Thermal Hydraulics Methods
TRAN	transition boiling
VERA	Virtual Environment for Reactor Applications
WEC	Westinghouse Electric Company

1. MILESTONE DESCRIPTION

The objectives of this milestone work are to assess improved capabilities of the multi-scale thermal-hydraulic (T/H) codes and models developed by the Consortium for Advanced Simulation of Light Water Reactors (CASL) for Departure from Nucleate Boiling (DNB) Challenge Problem (CP) (Reference 1), in accordance with the DNB CP implementation plan (Reference 2). The multi-scale models can range from fine mesh Computational Fluid Dynamics (CFD) simulation of flow field surrounding a fuel rod to a full core modeling of a Pressurized Water Reactor (PWR). The assessments are performed based on the CASL subchannel code COBRA-TF (CTF) (Reference 3) and the Computational Fluid Dynamics (CFD) code Hydra-TH (Reference 4).

DNB is one of the safety-related Challenge Problems (CP) that CASL is addressing in support of PWR power uprate, high fuel burnup and plant lifetime extension. DNB is also referred to as Critical Heat Flux (CHF), boiling crisis or burnout.

COBRA-TF (Coolant Boiling in Rod Arrays – Two Fluid) is a transient subchannel code based on two-fluid formulation that separates the conservation equations of mass, energy, and momentum to three fields of vapor, continuous liquid, and entrained liquid droplets. The code is being further improved by CASL as part of the Virtual Environment for Reactor Applications (VERA) multi-physics software package.

Hydra-TH is a CFD code based on a hybrid finite-element/finite-volume incompressible or low-Mach flow solver built using the Hydra toolkit. The current development version of Hydra-TH is capable of simulating rod bundle geometry under single-phase flow conditions, including turbulent mixing and flow distributions in rod bundles. Its capabilities for simulating two-phase flow conditions are under development.

1.1 Approach and Implementation

The approach to the milestone work is collaboration among the CASL Focus Areas and the partners, bringing together multi-disciplinary expertise with background in DNB phenomenology, T/H analysis, computer hardware and software, subchannel and CFD modeling and simulations. The following evaluations on the improved CASL T/H codes and models were performed under this milestone:

1) CTF model development and application for DNB prediction during Reactivity Insertion Accident (RIA) tests,

2) Application of the CTF code and its preprocessor to modeling and simulation of a PWR fuel assembly in transient calculations, and

3) Application of the Hydra-TH code to modeling and simulation of rod bundle geometry under single-phase flow condition.

1.2 Working Group

The working group consists of partners from the CASL Advanced Modeling Applications (AMA), Thermal-Hydraulic Methods (THM) and Physics Integration (PHI) Focus Areas, including the following contributors:

Name	CASL Focus Area	Affiliated Organization
Mark A. Christon	THM FA Lead	LANL
Lori Pritchett-Sheats	THM	LANL
Jozsef Bakosi	THM	LANL
Jin Yan	AMA	Westinghouse
Liping Cao	AMA Support	Westinghouse
Larry Hampshire	AMA Support	Westinghouse
Vefa Kucukboyaci	AMA Support	Westinghouse
Emre Tatli	AMA Support	Westinghouse
Yixing Sung	AMA	Westinghouse
Robert K. Salko	PHI	ORNL
Scott Palmtag	PHI FA Deputy Lead	ORNL
Hongbin Zhang	AMA	INL
Zeses E. Karoutas	AMA FA Lead	Westinghouse

2. CTF APPLICATION TO RIA DNB PREDICTION

2.1 General Description

CTF is being evaluated as part of the VERA multi-physics software package to help the nuclear industry address operational and safety challenge problems, such as DNB and RIA. In this section, CTF's capability for transient fuel rod and subchannel analyses including DNB prediction is evaluated by modeling and simulating power burst experiments with high burnup PWR fuel rods. These experiments were a series of tests performed using pulse irradiation to evaluate fuel rod failure with respect to fuel enthalpy, coolant conditions, and fuel rod design and power history during RIAs such as control rod ejection. Experiments have been modeled and simulated to evaluate CTF's predictive capability for DNB occurrence, fuel rod thermal response, and heat transfer from single-phase convection to post-CHF regimes during fast RIA transients.

2.2 Description of Test Cases

The Japan Atomic Energy Research Institute (JAERI) has conducted RIA-simulation tests in the Nuclear Safety Research Reactor (NSRR) facility on PWR fuel rods with burnup levels between 40 and 50 GWD/MTU. The PWR fuel segments were extracted from 17x17 PWR fuel rods previously irradiated in two different commercial reactors, Ohi (tests HBO 5-7) and Takahama (tests TK 1-7) 11-16 (References 5 and 6). Figure 2-1 shows a diagram of the test setup used in the pulse experiments. Specific to this study, experiments using the Takahama reactor fuel segments, which are also referred to as the TK tests, have been modeled and analyzed.

In the TK experiment series, test segments were taken from two fuel types. The main characteristics of the two fuel designs are provided in Table 2-1. The major differences are in the pellet diameter, cladding inner diameter, cladding wall thickness, and pellet length. The Type B pellet is slightly smaller than the Type A pellet. Thus, at the same linear power, the Type B pellet has the higher energy density than the Type A pellet.

Table 2-1: Clad and Fuel Pellet dimensions of the fuel segments used in the TK tests

Fuel Type	Clad OD (in.)	Clad ID (in.)	Clad Thickness (in.)	Gap Thickness (μm)	Pellet OD (in.)	Pellet Height (in.)
A	0.374	0.329	22.5	170	0.322	0.394
B	0.374	0.324	25.2	170	0.317	0.354

The locations of the TK segments in the parent rods are shown in the diagram in Figure 2-2. TK-1 and TK-6 were taken from the same parent fuel rod, which was removed from the fuel assembly after two cycles with an exposure of 38 GWD/MTU. The remaining specimens were taken from two other parent fuel rods that went through three cycles of operation. The majority of fuel rod segments for the TK tests were refabricated with pellet stack lengths of approximately 5.3-5.5inches (130-135mm), which is equivalent to 10 Type A pellets or 15 Type B pellets. Two segments, TK-5 and TK–6, were refabricated with shorter stacks of 4.3inch (110mm, or 11 pellets) each. All fuel segments were pressurized to 1atm (0.1MPa) with helium.

The TK PWR tests are characterized by narrow pulses, all less than 7msec of Full Width at Half Maximum (FWHM) and with the majority being 4.4msec FWHM. A plot of the power pulses used in the tests is shown in Figure 2-3. Among the seven TK tests, two segments failed before the peak fuel enthalpy was achieved. The remainder of the tests survived with enthalpies significantly higher than those that failed. Therefore, the test data seemed to indicate that rather than onset of DNB, the burnup-dependent condition of the cladding, e.g. stress, oxide thickness, fast neutron fluence (irradiation damage), and hydrogen content, is critical to the survival of the cladding.

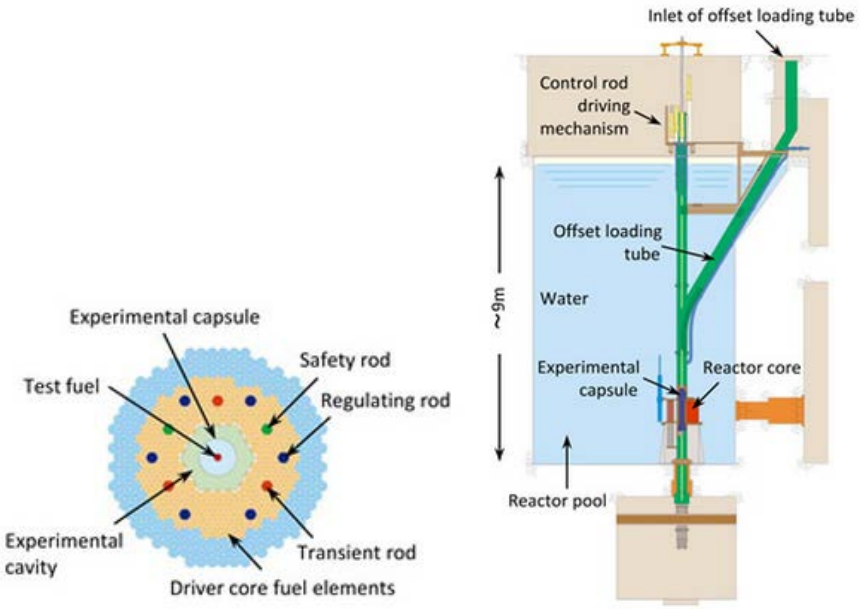

Figure 2-1: Simplified Diagram of Test Capsule Used in RIA Pulse Experiments (From: http://www.jaea.go.jp/english/04/ntokai/kasokuki/kasokuki_03.html)

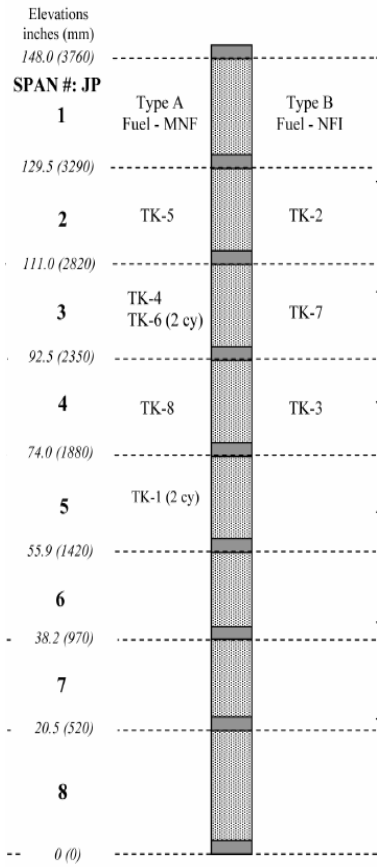

Figure 2-2: Locations of Test Segments Removed from Parent Rods

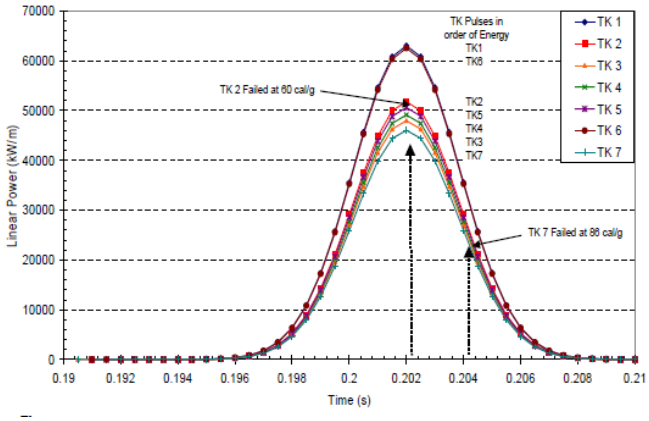

Figure 2-3: Linear Power as Function of Time in TK Tests

2.3 CTF Model and Input Description

The test sections are modeled as a single rod in a single channel. The fuel rod is divided into three axial zones, each zone with different number of axial nodes with the minimum axial nodal length of about 1.325inches (33.66mm) in the heated region. The first zone is the inactive bottom fuel length with two axial nodes, the second zone is the active fuel length with four nodes, and the third zone is the inactive top fuel length with two nodes, as shown in Figure 2-4.

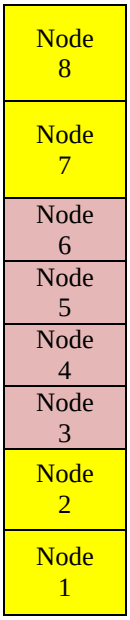

Figure 2-4: Axial Noding of TK Test Models

The channel flow area and perimeter are approximated as a square based on the inner diameter of the test capsule. The total axial length and active (heated) fuel length vary based on the type of test fuel. The axial lengths, channel flow area, and perimeter along with the fuel rod dimensions, are listed in Table 2-2.

Table 2-2: Axial Lengths, Channel, and Fuel Rod Dimensions

Fuel Type	Total Axial Length (in)	Heated Length (in)	Test Cases	Channel Flow Area (in^2)	Channel Perimeter (in)	Rod OD (in)	Rod ID (in)	Gap Width (in)	Clad Thickness (in)
A	12.244	5.3	TK-1, TK-6	6.311	8.905	0.374	0.322	0.0035	0.02244
Short A	11.417	4.3	TK-4, TK-5			0.374	0.322	0.0035	0.02244
B	12.480	5.5	TK-2, TK-3, TK-7			0.374	0.317	0.0035	0.02519

A uniform axial power profile is assumed in the fuel rods, given the short stack lengths. The fuel pellet is radially divided into 6 segments, and the clad region divided into 2 segments. A typical pellet radial power profile, shown in Table 2-3 below, is applied. The CTF code built-in UO_2 and Zircaloy material properties are used for the model. The dynamic gap conductance model is used for gap conductance, and the fuel pellet is assumed at 95% theoretical density.

Table 2-3: Pellet Radial Power Profile

r/r_o	Relative Power Factor
0.0000	0.8714
0.3817	0.9144
0.4975	0.9267
0.5901	0.9433
0.6698	0.9605
0.7408	0.9733
0.8056	0.9867
0.8656	1.0341
0.9216	1.0675
1.0000	1.4193

The TK tests were performed in pool conditions (i.e., no forced coolant flow) at atmospheric pressure. As such, the CTF model prescribes a close to zero flow boundary condition at the channel inlet of 82.4°F and the pressure of 14.7psia at the channel outlet. All of the heat is assumed to be generated in the fuel. The power level within the test setup was input as a function of the linear power generation rate over time. The nominal linear power is 10kW/ft. The power levels as a function of transient time are shown in Figure 2-5.

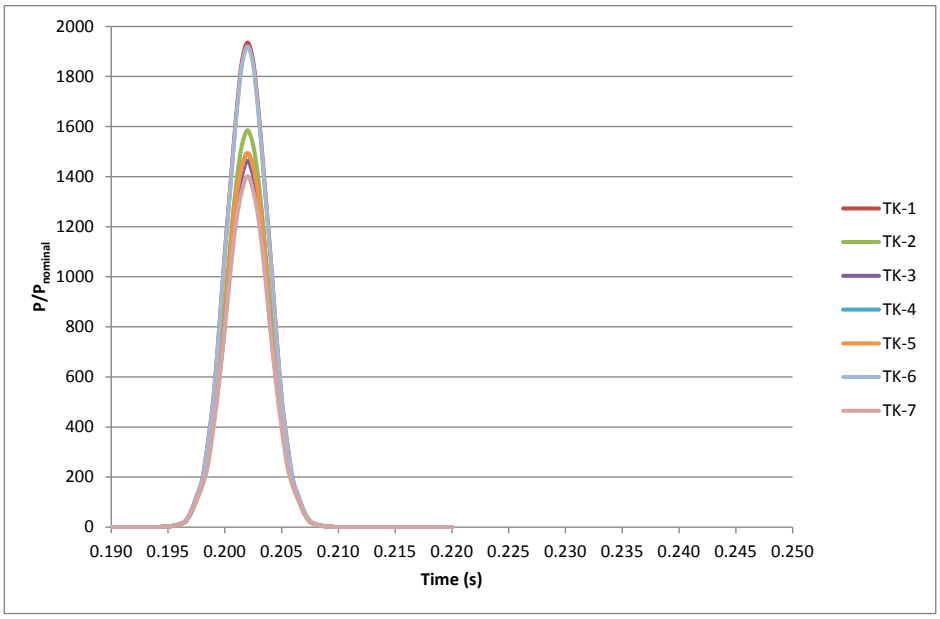

Figure 2-5: Power Input as Function of Time for Each TK Test Case

2.4 Results and Analysis

Test cases, TK-1 through TK-7 were run using CTF to predict DNB occurrences during the tests, as indicated by the DNB ratio (DNBR), given as,

$$DNBR = \frac{q''_{CHF}}{q''_{actual}}$$

Where q''_{CHF} is the predicted CHF by an empirical correlation and q''_{actual} is the measured local rod surface heat flux. DNB occurs when minimum DNBR (MDNBR) falls down to or below 1.0.

Figure 2-6 shows MDNBR calculated using the W-3 and the Biasi correlations available in the CTF code. Note that the time scale on each plot starts at 0.19seconds, consistent with the test results provided. The following observations can be made:

- In all cases, the MDBR plots show distinct periods with different slopes, corresponding to different heat transfer regimes that the system goes through, starting with single phase liquid (SPL), through subcooled boiling (SUBC), transition boiling (TRAN), and all the way to the post-DNB regime Inverted Annular Flow (IAF) as shown on Figure 2-6.

- Approach to critical heat flux or boiling crisis was indicated with the sudden change in the curves with a steep slope around 0.225seconds into the transient, when MDBR reaches or drops below 1.0.

- In cases with higher peak power, particularly TK-1 and TK-6, DNB was predicted to occur earlier by both W-3 and Biasi.

- W-3 correlation predicted DNB occurrence earlier than Biasi.

Figure 2-7 shows the fuel pellet rim temperatures for each case. The higher power cases, TK-1 and TK-6, resulted in the fuel temperatures at least 300°F higher than those of the other TK tests. Because the different DNB correlations affect only the clad temperatures, the pellet temperatures from these two cases are identical.

Significant difference between W-3 and Biasi correlations is observed in the cladding temperatures, as seen in Figure 2-8. CTF applies a modified Zuber ramp (Reference 8) to CHF in low flow conditions, i.e., pool boiling; however, this is only done when the default Biasi correlation is used. With the W-3 correlation, no such ramp is applied, leading to a prediction of the lower CHF, hence an earlier DNB occurrence. It is also observed that with the W-3 correlation, the heat transfer regime goes into the hot wall regime (IAF) after CHF was reached. In that regime, heat transfer from the clad to the coolant degraded beyond possibility of recovery to transition boiling regime. In the calculations with the Biasi correlation, the shorter period was observed in the IAF regime; however, most of the cases returned to transition boiling regime. The two high power cases TK-1 and TK-6 remained in the hot-wall regime later in the transient, but the cladding temperatures were predicted still lower relative to the W-3 calculations. Overall, one can conclude that the W-3 correlation, even without the Zuber ramp for pool boiling, yields conservative predictions of DNB occurrence.

Figure 2-9 shows the calculated heat fluxes as a function of the transient time. Because the calculated heat transfer coefficient was significantly smaller after the DNB occurrence as predicted by the W-3 correlation, the cladding surface heat fluxes were consequently smaller and the cladding temperatures were higher, as compared to those from the Biasi correlation. For the TK-1 and TK-6 cases with higher power peaks, onset of DNB occurred earlier than the other cases.

In order to assess the post-DNB predictive capabilities of CTF, the TK-2 transient run was extended to 10 seconds and the calculated temperatures and heat fluxes based on the W-3 and Biasi correlations were compared. Figure 2-10 compares the fuel pellet center, rim, and cladding surface temperatures, as well as the heat fluxes. Generally, there was no difference in the code-predicted temperatures until the onset of the DNB and diverge significantly during the post-DNB period. With W-3, the transient went into the hot-wall regime, resulting in very little heat transfer from the clad to the coolant. Much of the stored energy remained in the fuel pellet, leading to monotonically increasing pellet and clad temperatures. At ~9seconds, due to high temperatures and increased internal pressure, fuel relocation occurred, degrading the fuel pellet thermal conductivity. This manifested itself as the temperature bump seen in the pellet rim temperature. Because not much heat was transferred to the clad during that period, the clad temperature showed a temporary dip. With the Biasi correlation and its pool boiling correction, the transient remained in the transition boiling regime. Due to the relatively low fuel and clad temperatures, no fuel relocation was observed, and both the fuel and the clad temperatures were in a decreasing trend during the post-DNB period.

2.5 Summary

The TK experiments were modeled using the CTF code to assess its capability simulating an RIA test. The calculations demonstrated that CTF is able to simulate a fast transient with a large power pulse. DNB occurrence was predicted in all of the cases, after the power pulse, consistent with experimental observations. In the experiments, only two of the cases failed, one at the peak power, the other one after the peak power. The remaining cases survived with enthalpies significantly higher than those that failed while experiencing DNB occurrences as predicted by the DNB correlations. The CTF simulation results are consistent with the observed failures attributed to pellet-to-clad mechanical interaction (PCMI), rather than the DNB occurrence. The burnup-dependent condition of

the cladding, e.g. stress, oxide thickness, fast neutron fluence (irradiation damage), and hydrogen is deemed critical to the survival of the cladding under the RIA experiments. The flow-dependent mass and energy imbalance in CTF solutions were observed, especially after the end of the pulse. These imbalances were considered to be due to the zero flow condition, but had no effect on the results of the DNB predictions and conclusions.

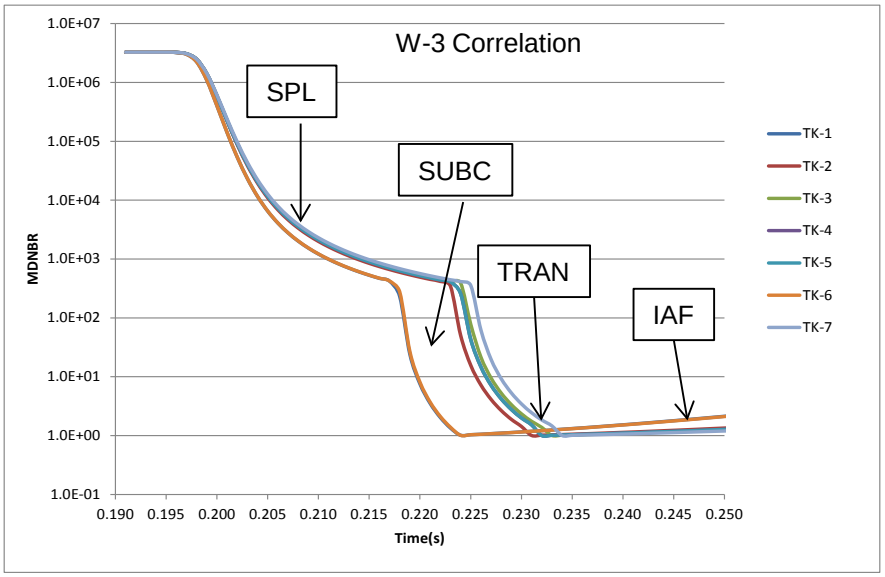

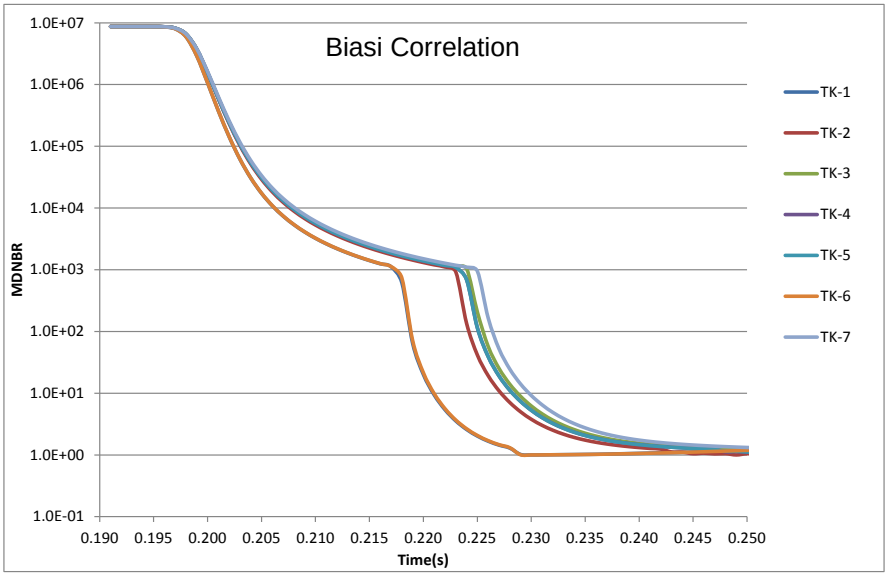

Figure 2-6: Minimum DNBR with W-3 and Biasi Correlations for Each TK Test Case

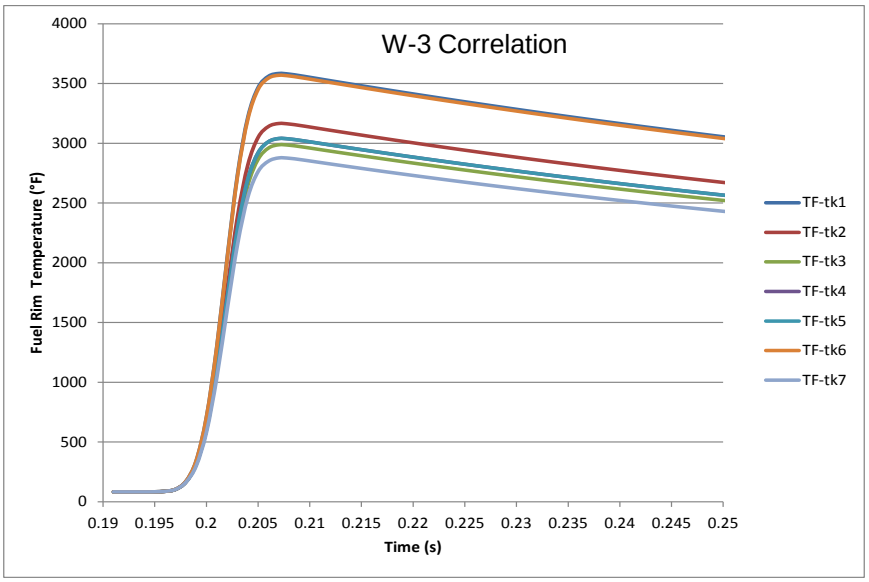

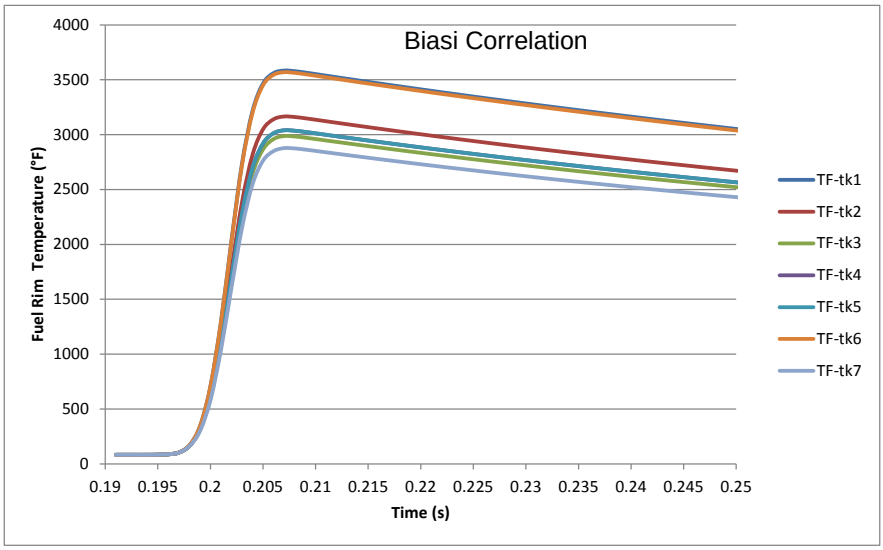

Figure 2-7: Fuel Pellet Rim Temperatures at Axial Mid-Point with W-3 and Biasi Correlations

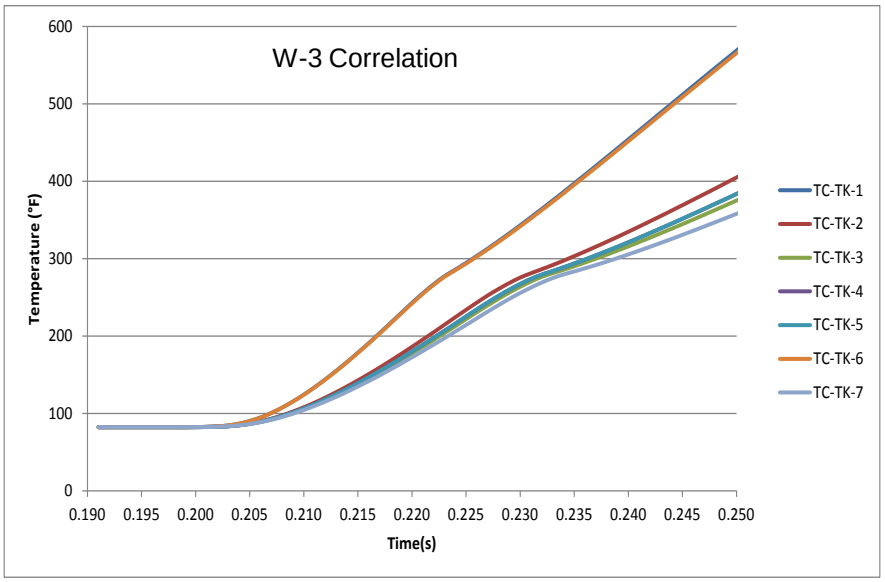

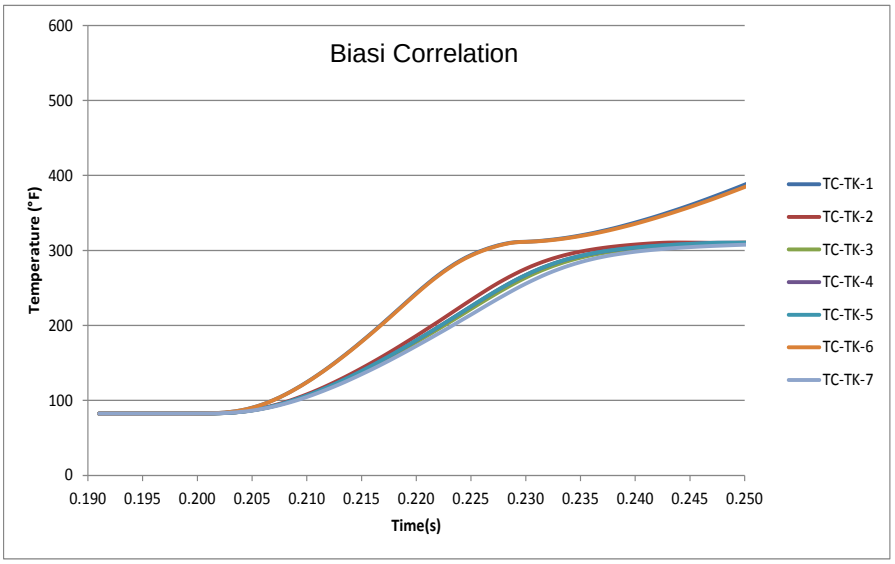

Figure 2-8: Clad Surface Temperatures at Axial Mid-Point with W-3 and Biasi Correlations

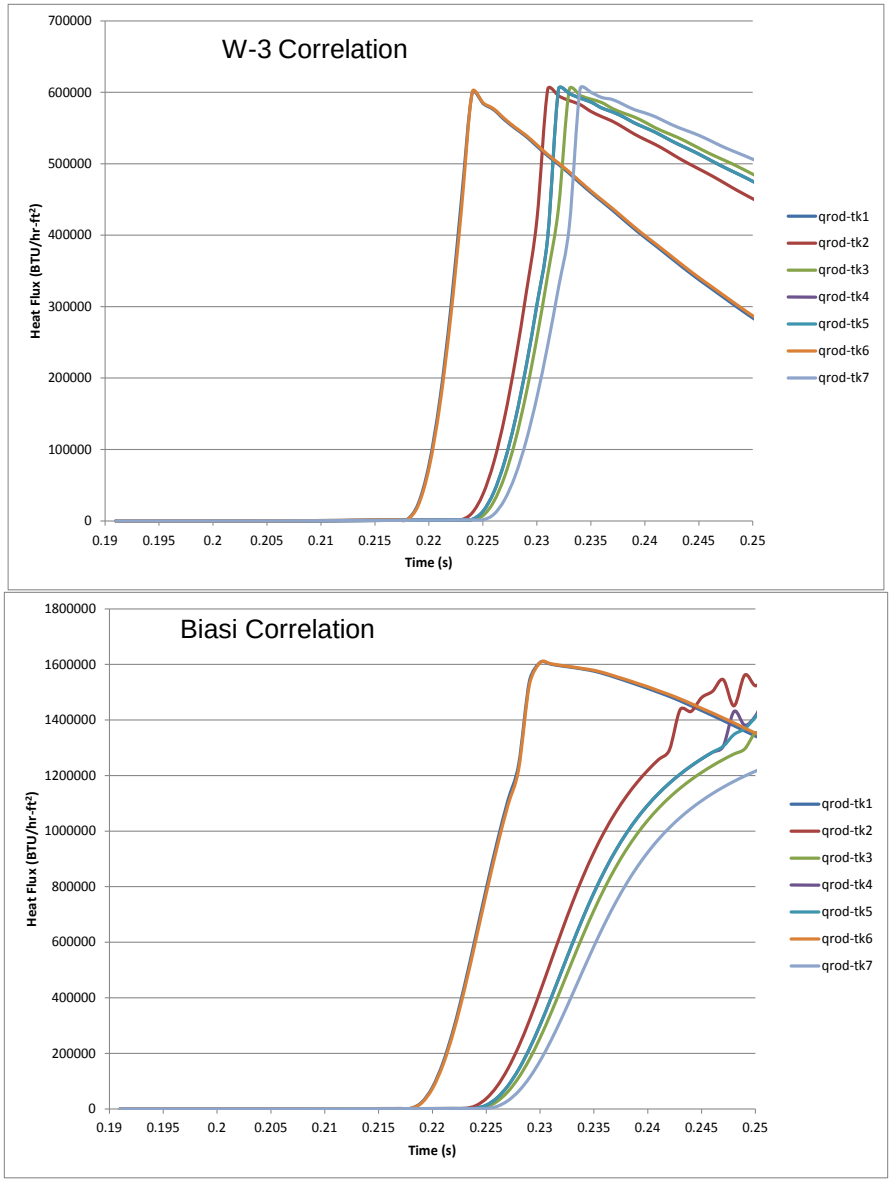

Figure 2-9: Heat Fluxes at Axial Mid-Point with W-3 and Biasi Correlations

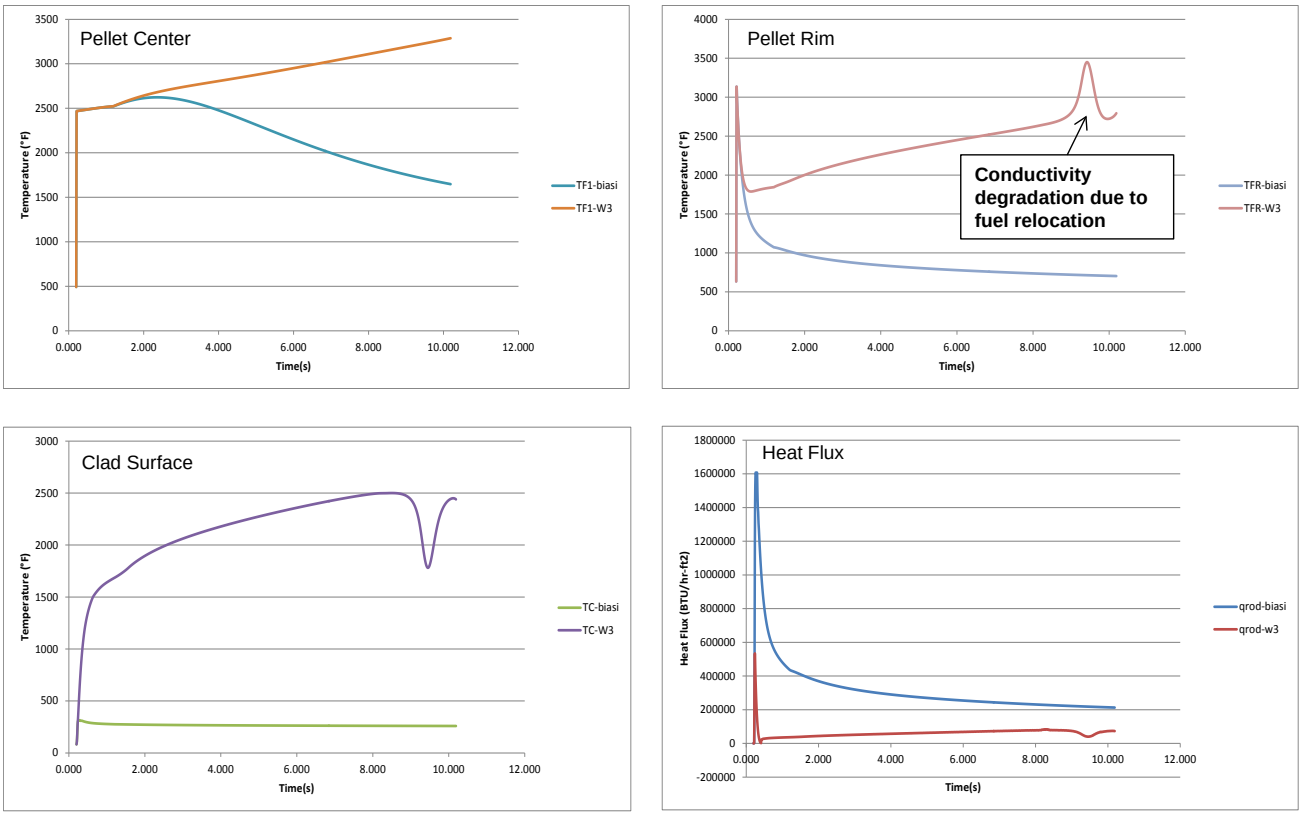

Figure 2-10: Comparison of Temperatures and Heat Fluxes for TK-2 Experiment

3. MODELING AND SIMULATION OF FUEL ASSEMBLY USING CTF

Based on the previous modeling of the 5x5 rod bundle geometry (Reference 9), the size and the complexity of the CTF model were increased to simulate an actual fuel assembly in transient calculations, in order to evaluate the adequacy of the model created by the preprocessor, to assess the capabilities and the performance of CTF with a large model, and to identify additional needs, capabilities, or areas for improvements of either CTF or the preprocessor. The full fuel assembly model is a precursor to a full core model for the DNB CP application.

3.1 Fuel Assembly Description

The current Westinghouse 17x17 fuel assembly design with a fuel rod outside diameter of 0.374inches (9.5mm), which is similar to the fuel assemblies used in Watts Bar Unit 1, was chosen for this study. There are 264 fuel rods, 24 guide tubes, and 1 instrument tube in this design, as seen in Figure 3-1. Eleven spacer grids including 6 mixing-vane (MV) grid spacers and 3 Intermediate Flow Mixer (IFM) grid spacers are located at certain elevations and inlet and outlet nozzles are at the bottom and top of the fuel assembly.

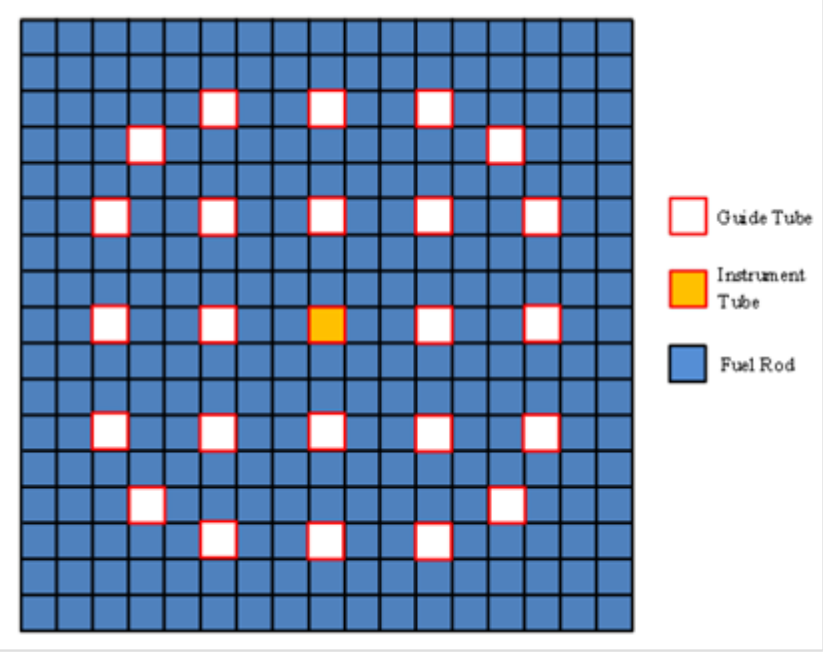

Figure 3-1: 17x17 Fuel Assembly Fuel Rod, Guide and Instrument Tube Pattern

Table 3-1 shows the design data, and Table 3-2 shows the initial operating and boundary conditions for the test problem modeled.

3.2 CTF Preprocessor Input

The CTF preprocessor was designed to create a CTF input deck for modeling rod-bundle geometry in a quick and less error-likely manner (Reference 7). The information supplied by the user to the preprocessor is basic data on assembly geometry, dimensions, axial locations of the grids, and axial and radial power distributions. Four input decks need to be supplied to the preprocessor and these are summarized below:

1. *control.inp* provides input options to select solution models, prescribe initial and boundary conditions, and time step size control, as well as convergence criteria.
2. *geo.inp* defines the assembly configuration, and global core wide geometry, as well as axial noding.
3. *assem.inp* is provided for each fuel assembly type to define fuel rod/guide tube/instrument tube dimensions, lattice pattern, and spacer grid locations and associated loss coefficients.
4. *power.inp* defines transient dependent radial and axial power profiles, as well as assembly and pin power factors.

When the preprocessor is run with the required input as outlined above, a CTF input file called *deck.inp* is created, ready to be run. When a parallel option is chosen, multiple CTF input files are created suitable for a multiprocessor run with assembly-based domain decomposition.

Table 3-1: Westinghouse 17x17 Assembly Design Description

Parameter	Unit	Value
Active Core Length	in	144
Rod Pitch	in	0.496
Clad Material		ZIRC
Clad Outer Diameter	in	0.374
Clad Thickness	in	0.0225
Fuel Material		UO2
Pellet Outer Diameter	in	0.3225
Guide Thimble Material		ZIRC
Guide Thimble Thickness	in	0.020
Guide Thimble Outer Diameter	in	0.482
Instrument Tube (IT) Material		ZIRC
IT Thickness	in	0.020
IT Inner Diameter	in	0.442
Assembly Pitch	in	8.466

Table 3-2: Initial and Boundary Conditions

Parameter	Unit	Value
Inlet Temperature	°F	544
System Pressure	psia	2250
Inlet Flow Rate	lb/s	178.054
Assembly Power	MW_{th}	22.465

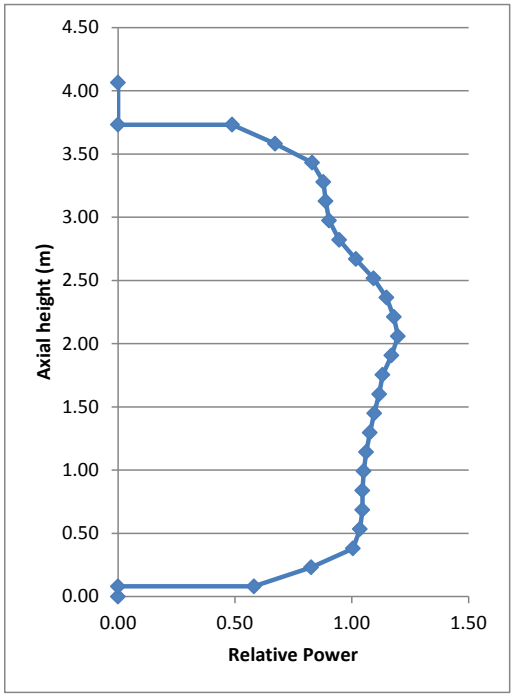

Figure 3-2: Axial Power Profile Used in 17x17 Fuel Assembly Model

3.3 CTF Assembly Model and Calculations

Using the CTF preprocessor and the data from Table 3-1, Table 3-2, and Figure 3-2, a full and a 1/8th symmetry assembly models, as shown in Figure 3-3, were created. The full assembly model had 324 channels, 612 gaps, 264 fuel rods, and 25 GT/IT, while the 1/8th assembly model had 45 channels, 72 gaps, and 45 fuel rods, 6 GT/IT. The fuel rod model used 6 radial nodes in the pellet and 2 in the clad, and 151 axial nodes. The average linear heat rate was set to 5.83kW/ft. A constant pellet-to-clad gap conductance was used in the fuel rods. A uniform assembly radial power distribution was assumed. The convergence criteria were set to default values, while the minimum time step size (DTMIN) and maximum time step size (DTMAX) were set to 1E-06 and 1.E-01, respectively.

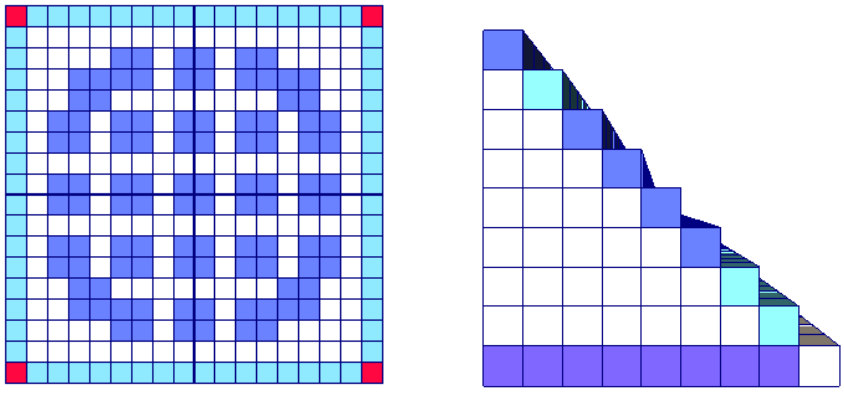

Figure 3-3: Full and 1/8th Symmetry Assembly Models

All simulations were performed with the CTF code and processors installed on the Westinghouse computer system **binford**, built and dedicated to the CASL development, testing, and applications. The login node on *binford* has 32 Intel Xeon E7- 8837 CPUs at 2.67GHz, with 1TB RAM. The compute nodes have a total of 1152 Intel Xeon X5670 CPUs, running at 2.93GHz, and with 4GB RAM per CPU. The CTF code and processors on binford were tested and verified using the existing test matrix for the VERA software installation.

3.3.1 Steady-State Runs

CTF employs an assembly-based domain decomposition/parallelization, requiring single assembly simulations run in serial mode. As such, using a single node of *binford*, the full assembly model reached steady-state in 672 time steps and 1.017seconds transient time. The total CPU/Wall Clock time was 1h 56m 21s. Similarly, the $1/8^{th}$ model reached steady-state in 642 time steps and 1.011seconds transient time. The CPU time/Wall Clock time for the $1/8^{th}$ model was 5m 22s. Steady-state solution of the whole assembly is shown in Figure 3-4 for liquid enthalpy, pressure, liquid density, and liquid velocity in the assembly sub-channels. The plots indicate that steady-state results are consistent with the expectations. The computing performance of the whole assembly model, however, requires improvement, perhaps by extending the assembly-based parallelism to utilize multiple CPUs in pressure matrix solution of a single assembly or other data parallelism schemes to speed-up the do-loop computations.

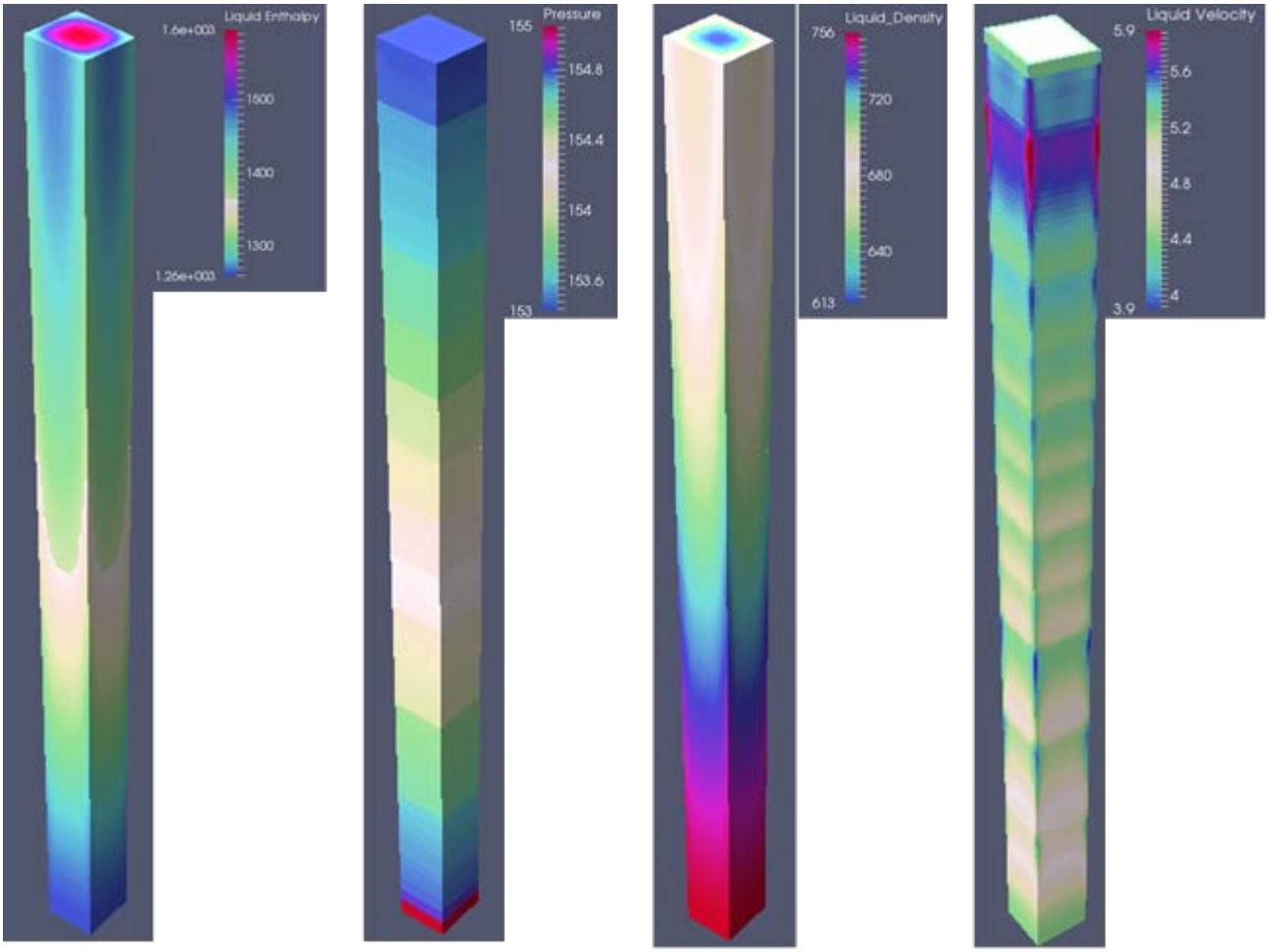

Figure 3-4: Steady-State Results of Full Assembly Calculations

A series of sensitivity calculations was performed to assess the performance of the full assembly model. It was determined that significant performance improvements were gained simply by switching to ISOL=3 or ISOL=5 and by changing NC from 3 to 1. This enabled the Krylov solver to be used to solve the pressure correction matrix and conduction to be considered in the radial direction of the rod only, respectively. With switching to the Krylov solver, the total CPU time dropped to 47m 23s, and switching to 'radial conduction only' reduced the CPU time even further to 20m 50s.

3.3.2 Transient Runs – HFP Rod Ejection Transient

A 5-second rod ejection transient initiated at Hot Full Power (HFP) was performed using the power forcing function in Figure 3-5. Once the steady-state convergence was achieved, the transient run was initiated using the *restart.in.crs* dump file created at the end of steady-state. Array allocation issues were identified with CTF in the restart mode, preventing the code to successfully perform a restart calculation. To speed-up code debugging, the 1/8th model was used in those calculations.

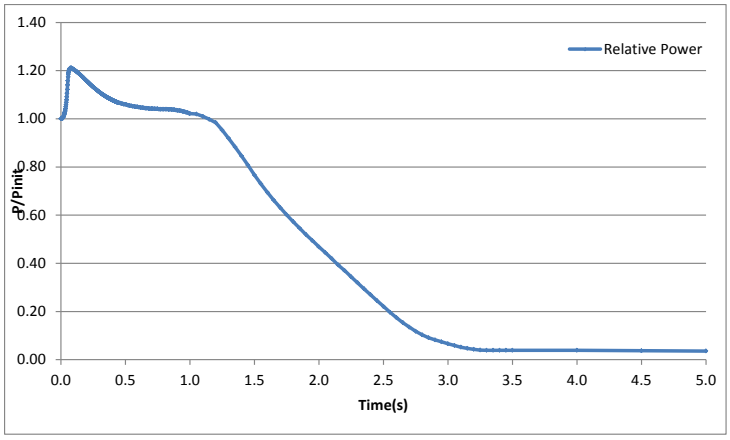

Figure 3-5: Power transient due to a Rod Ejection at HFP

A workaround was found in the form of performing the steady-state and the transient calculations in a single run, eliminating the need for a restart. The power forcing function in Figure 3-5 was expanded to include a 5 second pre-transient period with a nominal power of 1.0. In this pre-transient stage, the system achieved convergence and then the rod ejection scenario was imposed.

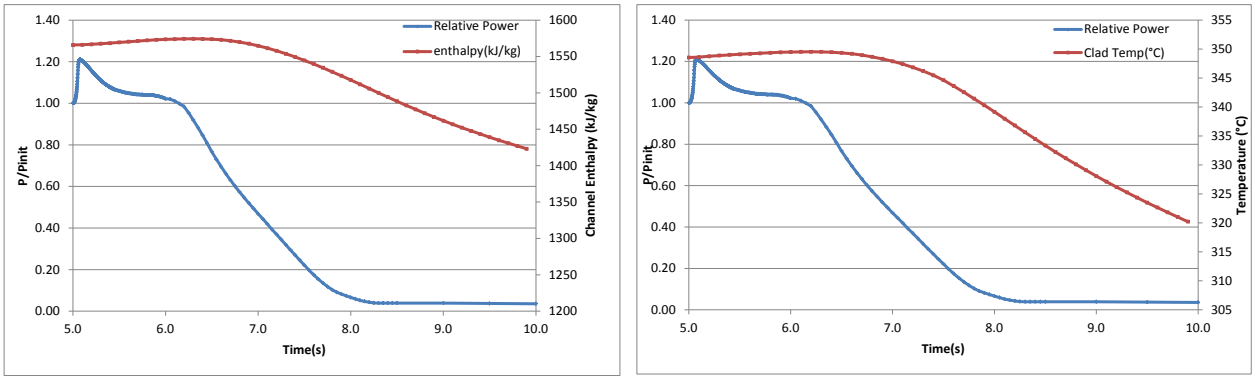

Figure 3-6: Enthalpy and Clad Surface Temperature Change during Rod Ejection at HFP

Figure 3-6 shows the liquid enthalpy and clad surface temperature behavior during the rod ejection transient. Because the transient is initiated at hot-full power conditions, the peak power was reached only 120% of the nominal power; therefore, the increase in the maximum clad temperature was only

~5°C. It was confirmed that the same transient calculation using the VIPRE-W code (Reference 10) resulted in a similar increase in clad surface temperature.

3.4 Summary

A full assembly model and a 1/8th symmetry model of the Westinghouse 17x17 fuel assembly were created using the CTF preprocessor for steady-state and transient calculations. The CTF preprocessor was found to be very helpful in greatly reducing the model creation effort and minimizing human error. Both the steady-state and transient predictions were found to be acceptable. Initial CTF calculations with the full model required extensive CPU time. It was found that with few simple input option changes, such as switching to Krylov solver from direct matrix inversion and eliminating the axial and azimuthal conduction solution, the CPU time was reduced to ~20 minutes on the Westinghouse compute system. It will however still be greatly beneficial to implement additional parallel processing capability within a single assembly to further speed-up the calculations. Additional needs/issues were identified with the preprocessor and CTF and these were communicated to the CASL team for further investigation and resolution.

4. HYDRA-TH SIMULATION OF ROD BUNDLE MIXING TEST

4.1 Introduction

This section summarizes the completed development work, challenges encountered, and the results obtained along the way in modeling a rod bundle with grid spacers using the Los Alamos National Laboratory (LANL) developed thermal-hydraulics CFD code Hydra-TH (References 4 and 12). The CFD analysis investigates thermal mixing inside the bundle, and the results will be used for the DNB CP Applications.

CFD analyses to investigate the thermal mixing were performed using two codes: the commercial code STAR-CCM+ version 7.06.012 by CD-adapco (Reference 13) and the CASL Hydra-TH code (build date 11/19/2013). With the years of Westinghouse experience behind it, STAR-CCM+ was used as the benchmark code to establish baseline CFD capability for comparisons with Hydra-TH results. Two CFD models were assessed: the smaller single span 3x3 subchannel model for quicker code debugging and parameter settings, and the six grid-span 5x5 rod bundle model (which has approximately 40 times more number of computational cells than the 3x3 model). Steady state single phase flow simulations were conducted for both models. Results from both Hydra-TH and STAR-CCM+ were compared for the 3x3 subchannel model. Temperature and velocity magnitude contour plots were presented across different post-processing cut planes. It should be noted that the code comparison is not intended for qualification or validation of the numerical solutions, but for determination of code capabilities, and showing progress in the continuing code and model development including the planned 5x5 rod bundle analysis. Although STAR-CCM+ results are available and show good agreement with experimental results for the 5x5 rod bundle model, the evaluation will be performed later when the Hydra-TH results become available.

4.2 Analysis Procedure

The singlespan 3x3 subchannel model is shown in Figure 4.2-1. The solid model was built in SolidWorks (Reference 14) according to the Westinghouse provided drawings and documents. Necessary clean-up was performed to remove small gaps, small edges and unimportant small features in the CAD models. Fluid domains were then extracted from the solid models by Boolean operation. The detailed modeling specifications are described in a proprietary document provided by Westinghouse (Reference 17) in accordance with the Non-Disclosure Agreements (NDA). The analysis procedures followed for both Hydra-TH and STAR-CCM+ in this report are given in Figure 4.2-2.

Figure 4.2-1: The 3x3 sub-channel model (fluid domain shown)

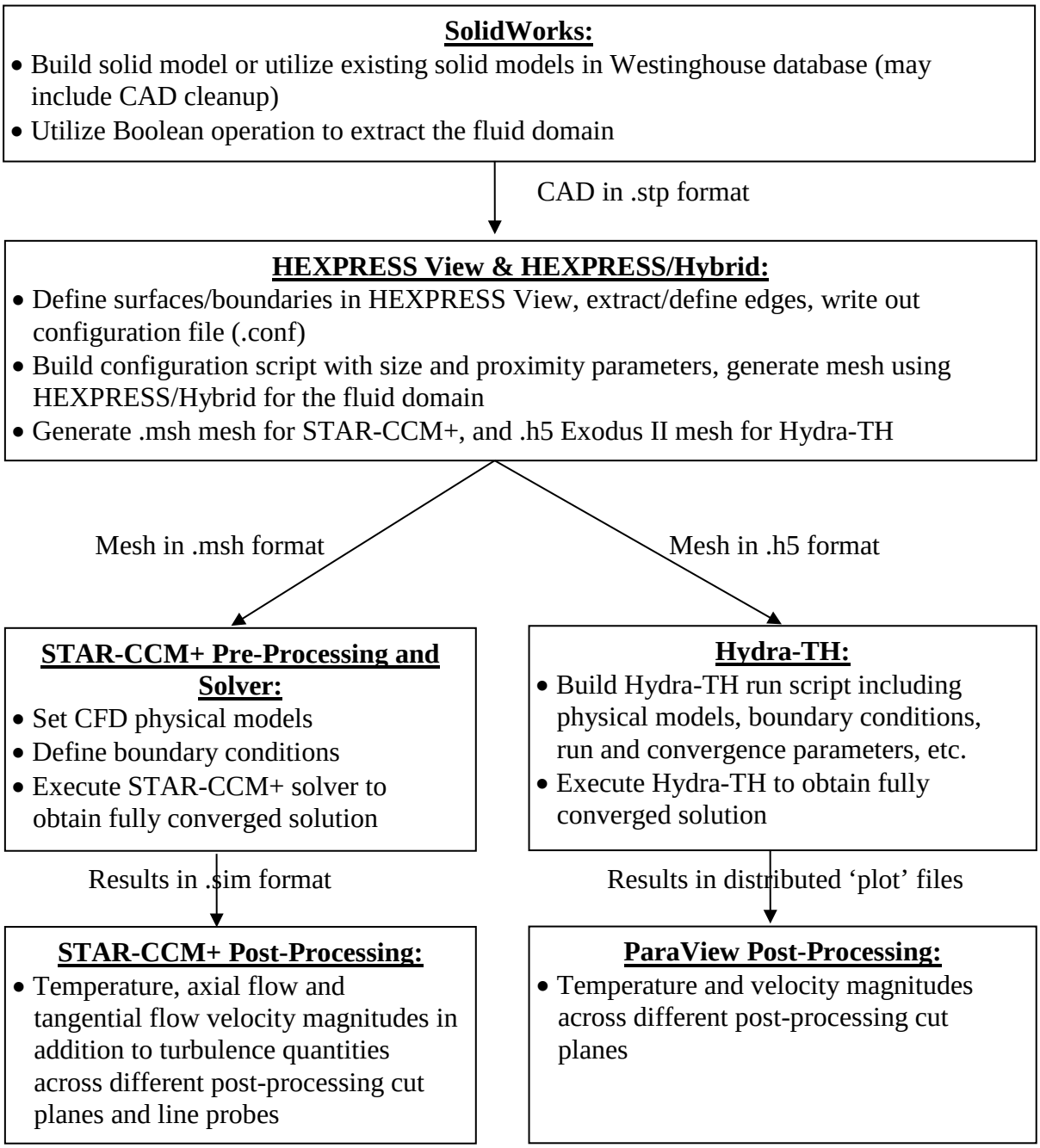

Figure 4.2-2: CFD analysis flow chart

4.3 Geometric Modeling

The single span 3x3 subchannel model was built and used to enable faster iterations when debugging and learning the intricacies of the codes that were being built and used for the first time in Westinghouse. The 3x3 subchannel model is not cut out from a 5x5 rod bundle, but is a separate model with the same level of detail representative of the 5x5 model. It has approximately 40 times less number of computational cells than the 5x5 rod bundle model. Figure 4.3-1 shows the 3x3 subchannel model.

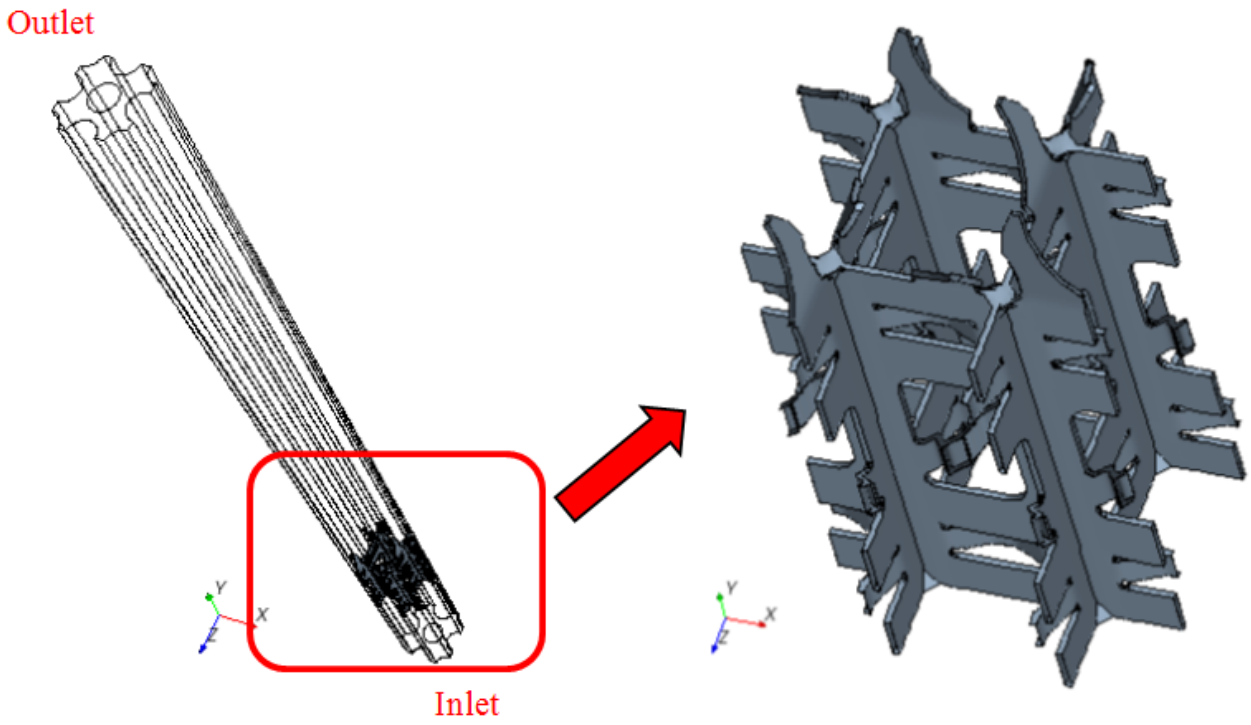

Figure 4.3-1: 3x3 sub-channel model

4.4 Computational Mesh

NUMECA HEXPRESS/Hybrid version 3.1_1 (Hexpress/Hybrid) (Reference 15) was utilized to generate the computational meshes for STAR-CCM+ and Hydra-TH for the 3x3 model. Hexpress/Hybrid is a parallel unstructured hexahedral dominant mesh generator for complex and/or unclean geometries, with capability to add high quality prism layers. There are still minor bugs within the software that are being communicated back to NUMECA as they are discovered during the model development (such as such as jumping over features that are clearly captured elsewhere in the mesh, commented in some figures below).

Note: When generating .h5 format meshes using Hexpress/Hybrid, 'FileName_idmap.txt' file is written out which includes the sideset ID's for the model boundaries which are required for the Hydra-TH run script when specifying boundary conditions.

A single Hexpress/Hybrid configuration script was built for both Hydra-TH and STAR-CCM+ meshes, only the output file format has been changed for the different format meshes for the different solvers (.h5 Exodus II format for Hydra-TH and .msh format for STAR-CCM+). The two generated meshes thus were exactly the same, with the below properties:

****

Mesh info
Number of hexahedrons: 6505707
Number of tetrahedrons: 68292
Number of prisms: 1010857
Number of pyramids: 251025
Number of cells: 7835881
Number of vertices: 7754710
Number of patches: 1271906
Number of selections: 10

****

Mesh Quality
MaxRatio: 0.99759
MaxRatio Celltype: 4
Num cells with ratio > 0.95: 270
Num cells with ratio > 0.9: 1548
Num negative jacobian: 0
Num concave cells: 0
Num twisted cells: 0
Num negative cells: 0
Minimal edge-length: 3.26534e-06
Average edge-length: 0.000200125
Maximal edge-length: 0.000640661
Max equiangular skewness: 0.958853
Max adjacent volume ratio: 86.4819
Max expansion ratio: 20.1691

****

Both format meshes had 7,835,881 computational cells. Figures 4.4-1 through 4.4-3 depict the mesh densities.

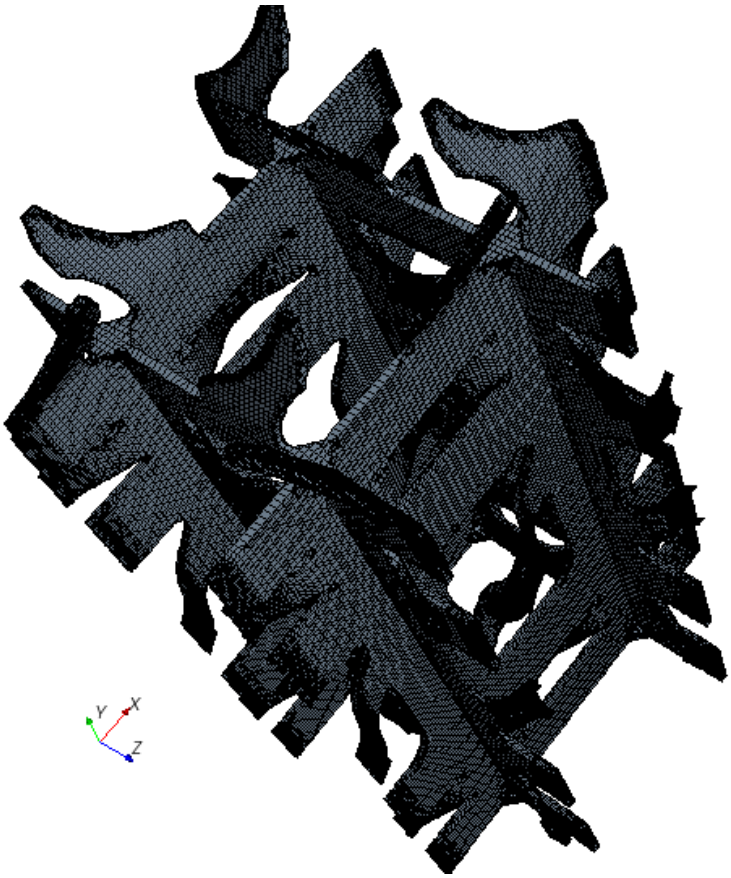

Figure 4.4-1: Mesh density on the grid for the 3x3 model

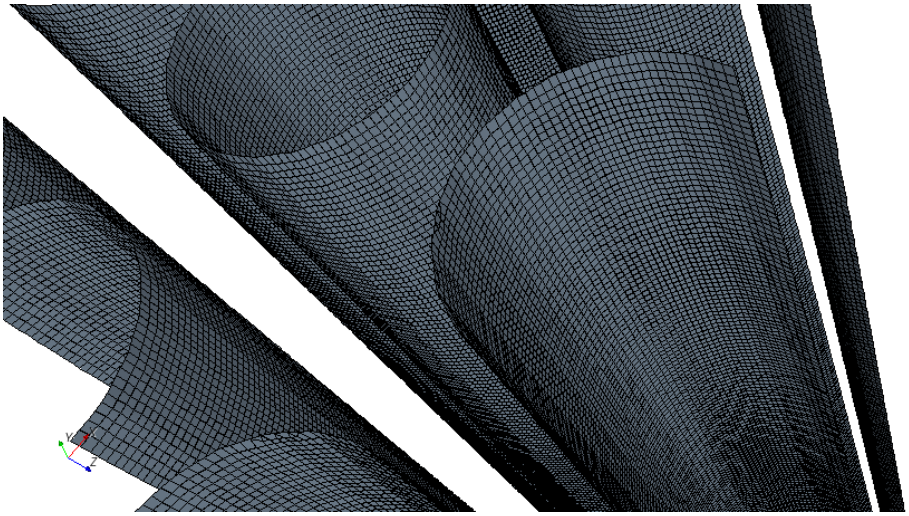

Figure 4.4-2: Mesh density on the rods for the 3x3 model

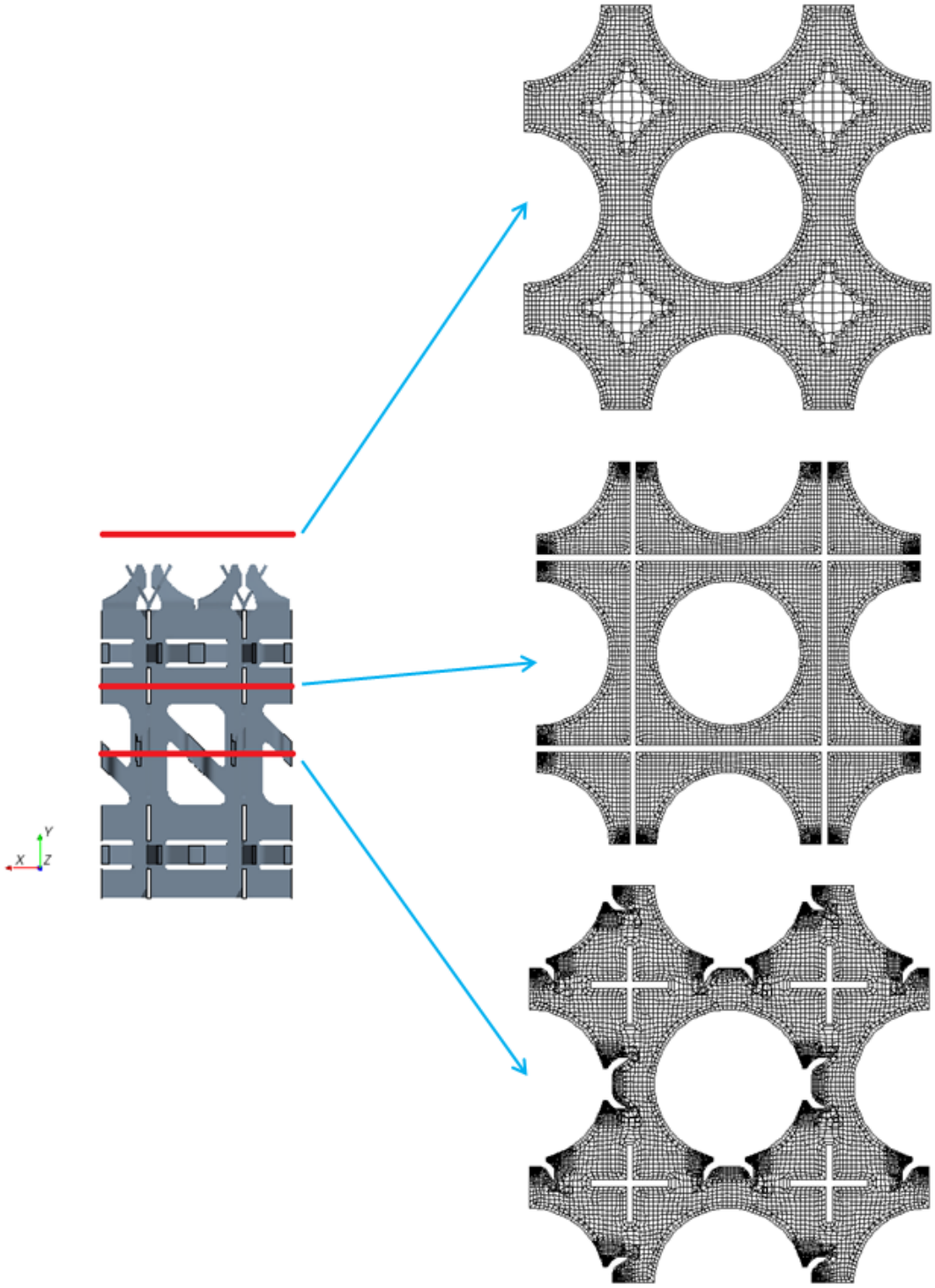

Figure 4.4-3: Mesh density on the horizontal cut planes for the 3x3 model

4.5 Model Setup and Run Convergence

4.5.1 Boundary/Flow Conditions

Only the fluid domain was modeled in all cases presented herein. An important note is that Hydra-TH currently does not have the capability for prescribing temperature dependent fluid properties, thus constant properties were utilized both in Hydra-TH and STAR-CCM+ simulations. This is of course not representative of real world conditions, but the decision was made to follow this path in order to be consistent with the codes. A STAR-CCM+ case with temperature dependent properties will be run and the differences will be noted. Single phase steady-state flow was prescribed, and the energy equation was solved with both codes.

The SIMPLE algorithm with relaxation values is used to couple the equations in STAR-CCM+ and realizable k-ε two-layer all y+ wall treatment turbulence models were implemented for this run. Projection algorithm with backward Euler is used to couple the equations in Hydra-TH, and RNG k-ε was utilized for this run. The fluid conditions and properties are listed in Table 4.5-1 below.

Table 4.5-1: Coolant Properties

Reference Pressure (psi)	2319.719
Density (kg/m^3)	780.25
Specific Heat (J/kg-K)	4943.3
Thermal conductivity (W/m-K)	0.61043
Dynamic viscosity (Pa-s)	1.0024E-4

The boundary conditions for the 3x3 model are presented in Table 4.5-2 below (for both codes).

Table 4.5-2: Boundary Conditions of the 3x3 Model for Both Codes

Boundary Group	Location	Boundary Condition
Inlet	Inlet in Figure 4.3-1	Velocity inlet with V_{normal} = 4.655696 m/s and T_{inlet} = 270.902 °C
Outlet	Outlet in Figure 4.3-1	Pressure outlet (0 psi), T_{static} = 270.902 °C
Hot rod	Center rod in Figure 4.3-1	No-slip wall, uniform heat flux prescribed on OD surface = 713870.0 W/m^2
Cold rods	Peripheral partial rods in Figure 4.3-1	No-slip wall, uniform heat flux prescribed on OD surface = 591279.7 W/m^2
Grid	Shown in Figure 4.3-1	No-slip wall, adiabatic
Side walls	Side cut planes in Figure 4.3-1	No-slip wall, adiabatic

4.5.2 Run Convergence

All models were run until steady-state convergence was achieved. The residuals plots and the monitors are presented in this section.

STAR-CCM+

Total of 1000 iterations were run, but as seen below from Figure 4.5-1, stability is reached at approximately 800 iterations.

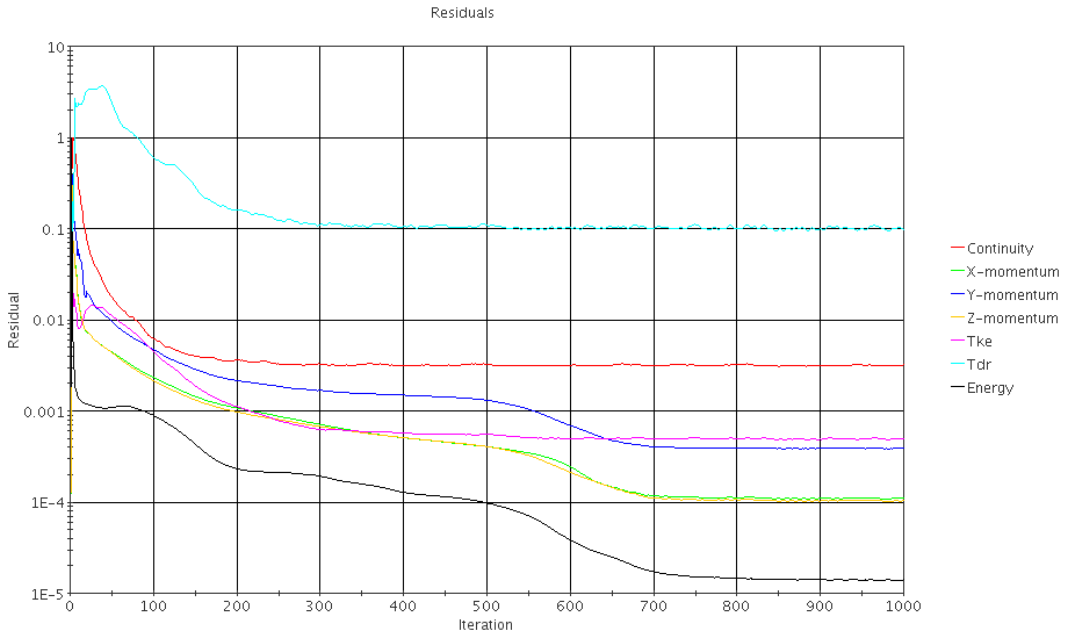

Figure 4.5-1: STAR-CCM+ 3x3 model residuals

At iteration number 1000 (last iteration), the residual values were as below:

- Continuity 0.0032
- X-momentum 1.0996E-4
- Y-momentum 3.8589E-4
- Z-momentum 1.0471E-4
- Turbulent kinetic energy (Tke) 4.8877E-4
- Turbulent dissipation rate (Tdr) 0.09726
- Energy 1.4042E-5

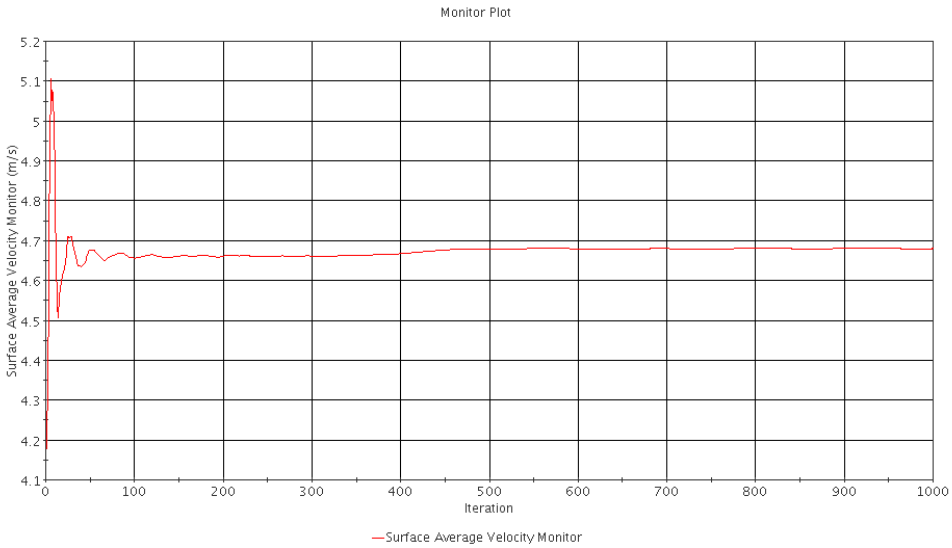

Figure 4.5-2: STAR-CCM+ 3x3 model area averaged velocity at the outlet

At iteration number 1000 (last iteration), the area averaged velocity at the outlet was 4.6788 m/s.

Hydra-TH

The code was run for 25000 time steps, but as seen below from Figures 4.5-3 and 4.5-4, stability is reached at approximately 12000 time steps.

Area averaged velocity and temperature data at the domain outlet were printed out from the Hydra-TH run and presented below showing run convergence. The error norms were not available for the projection strategy but at steady-state, all the residuals are expected to be at or below the convergence criteria of the linear solvers (1.E-3).

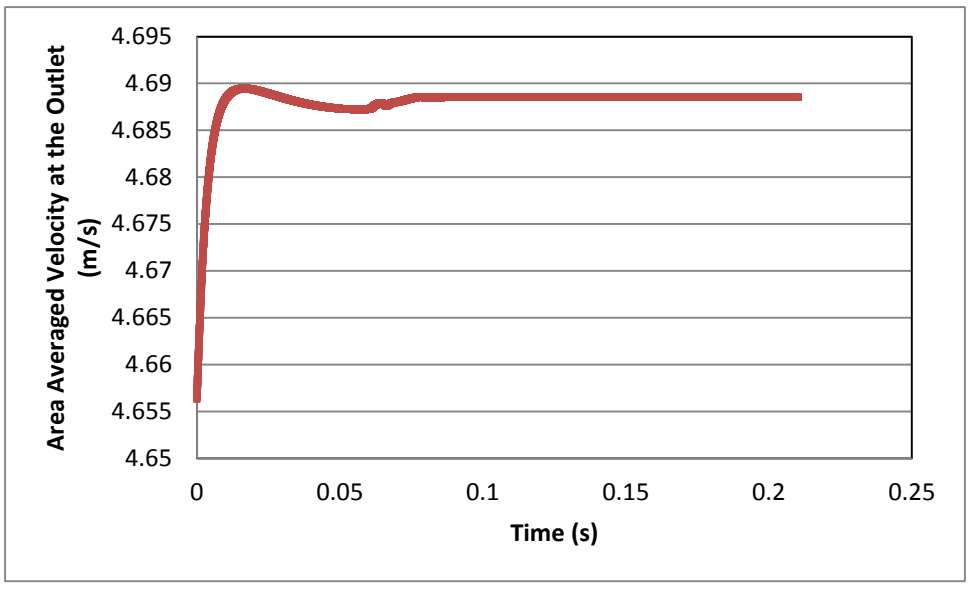

Figure 4.5-3: Hydra-TH 3x3 model area averaged velocity at the outlet

At the last time step, the area averaged velocity at the outlet was 4.6885 m/s.

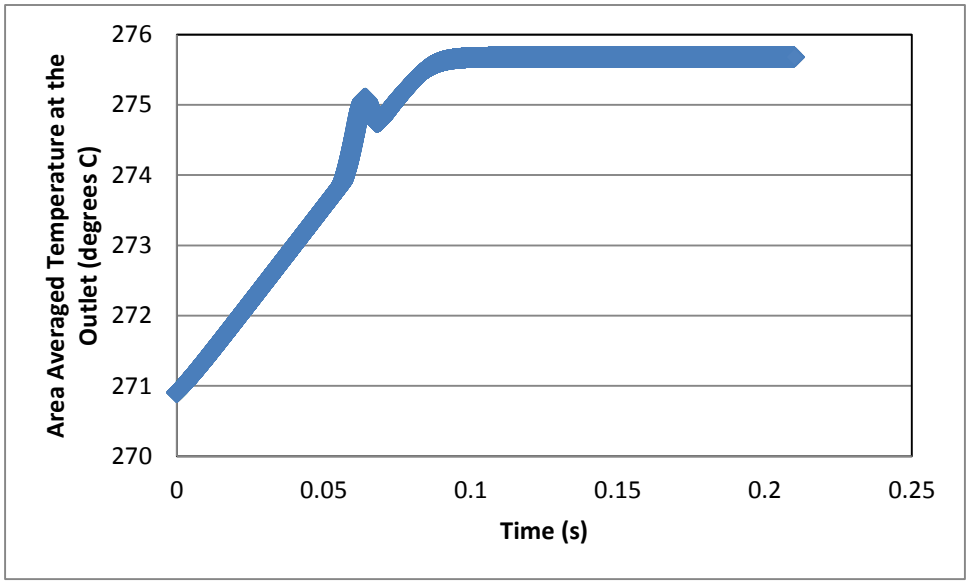

Figure 4.5-4: Hydra-TH 3x3 model area averaged temperature at the outlet

At the last time step, the area averaged temperature at the outlet was 275.679 °C.

4.6 Post-Processing of Results

Kitware ParaView (Reference 16) is the preferred post-processing software for Hydra-TH and version 4.1 is being used at Westinghouse.

Velocity Magnitude Results

Velocity magnitudes are presented for the Hydra-TH and STAR-CCM+ codes across horizontal cut planes at elevations Y = - 0.019 m, Y = 0 m and Y = 0.017 m in addition to one vertical cut plane at X = 0 m.

Figures 4.6-1 through 4.6-3 show the velocity magnitude contour plots across the horizontal cut planes, and Figure 4.6.1-4 shows the velocity magnitude contour plots across the vertical cut planes.

Temperature Results

Temperatures are presented for the Hydra-TH and STAR-CCM+ codes across horizontal cut planes at elevations Y = - 0.019 m, Y = 0 m and Y = 0.017 m.

Figures 4.6-5 through 4.6-7 show the temperature contour plots across these horizontal cut planes.

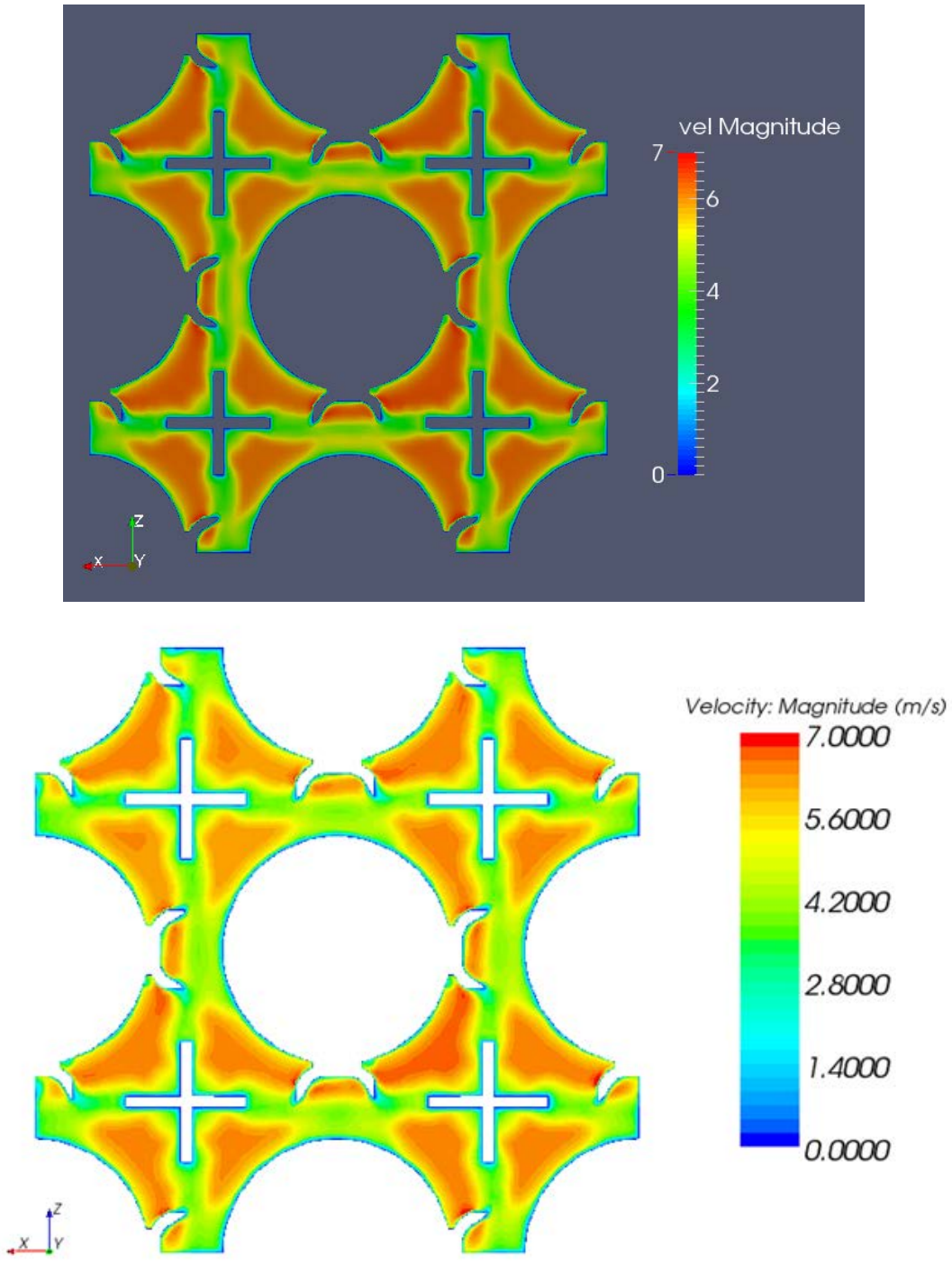

Figure 4.6-1: Velocity magnitude on horizontal cut plane at Y= - 0.019 m for Hydra-TH (top) and STAR-CCM+ (bottom)

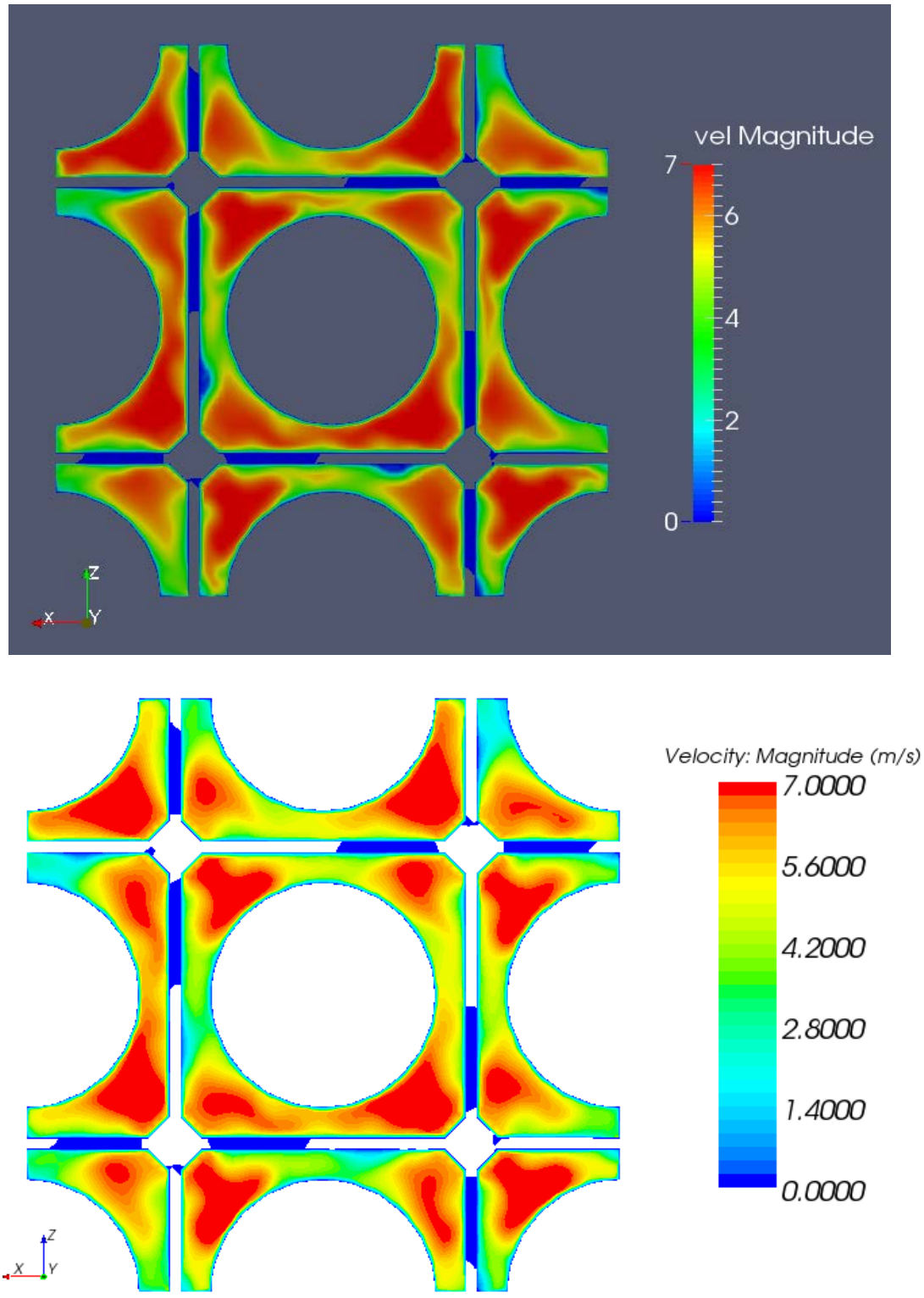

Figure 4.6-2: Velocity magnitude on horizontal cut plane at Y=0 m for Hydra-TH (top) and STAR-CCM+ (bottom)

(note the blue regions where the mesher jumped over the grid solid; more visible in Figure 4.6-6)

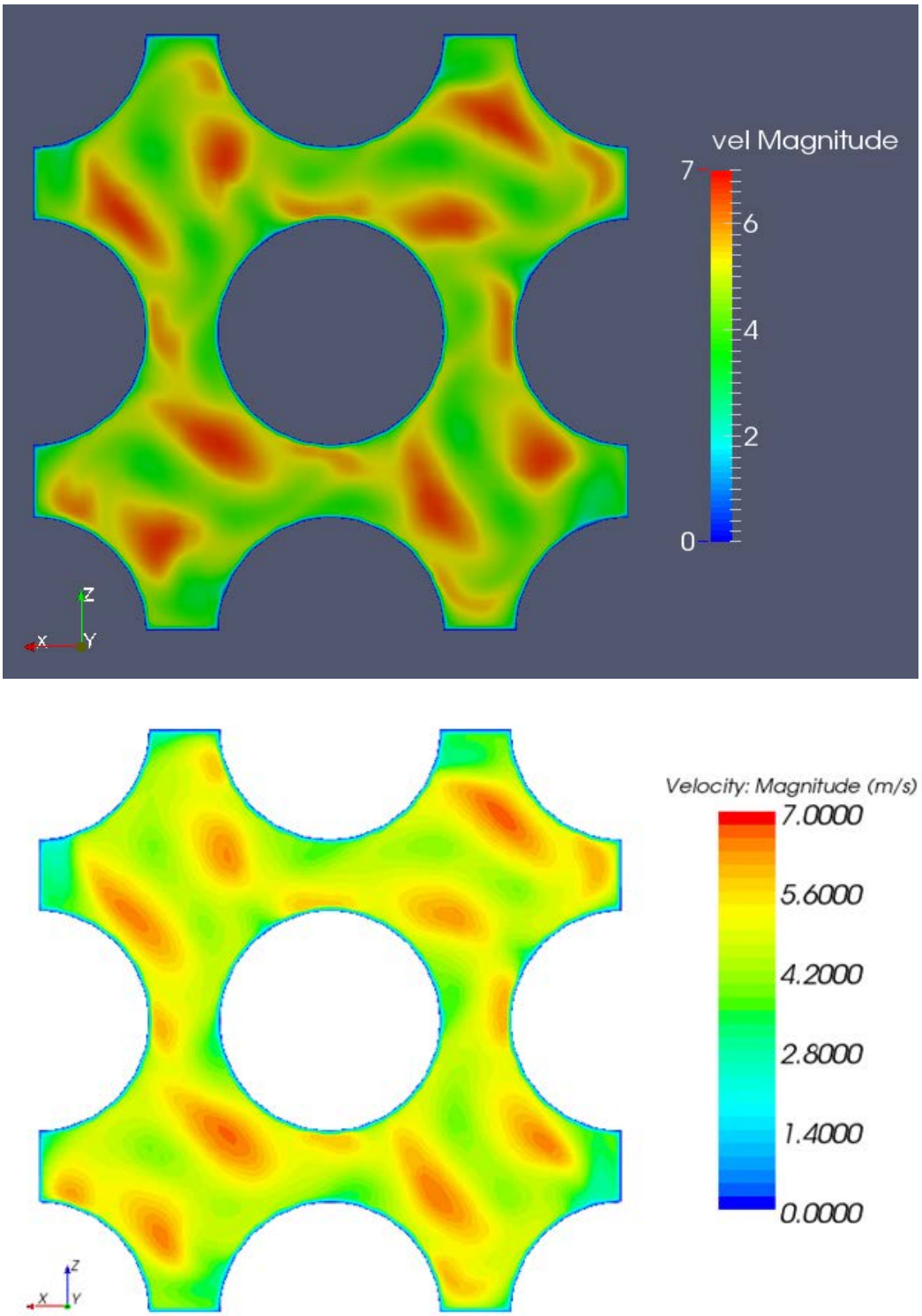

Figure 4.6-3: Velocity magnitude on horizontal cut plane at Y= 0.017 m for Hydra-TH (top) and STAR-CCM+ (bottom)

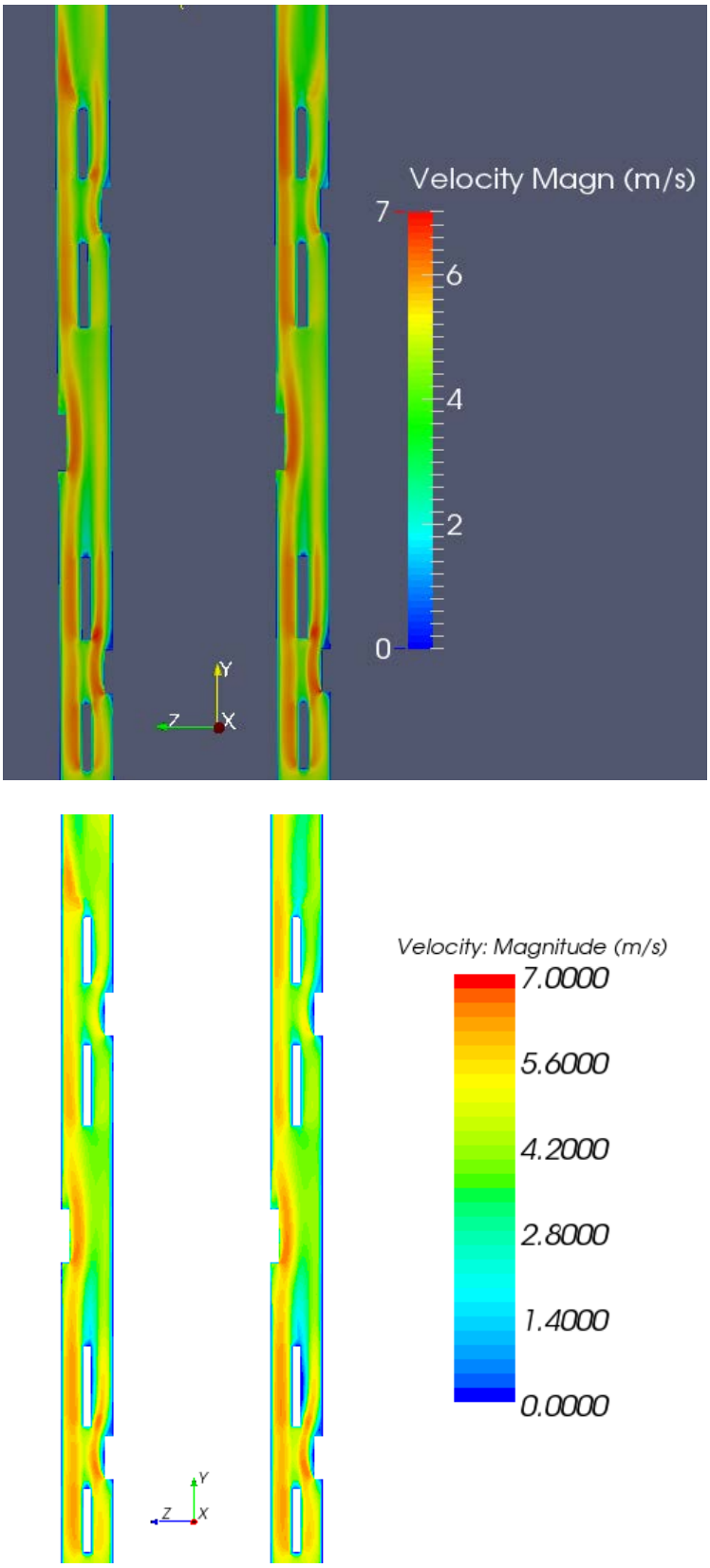

Figure 4.6-4: Velocity magnitude on vertical cut plane at X= 0 m for Hydra-TH (top) and STAR-CCM+ (bottom)

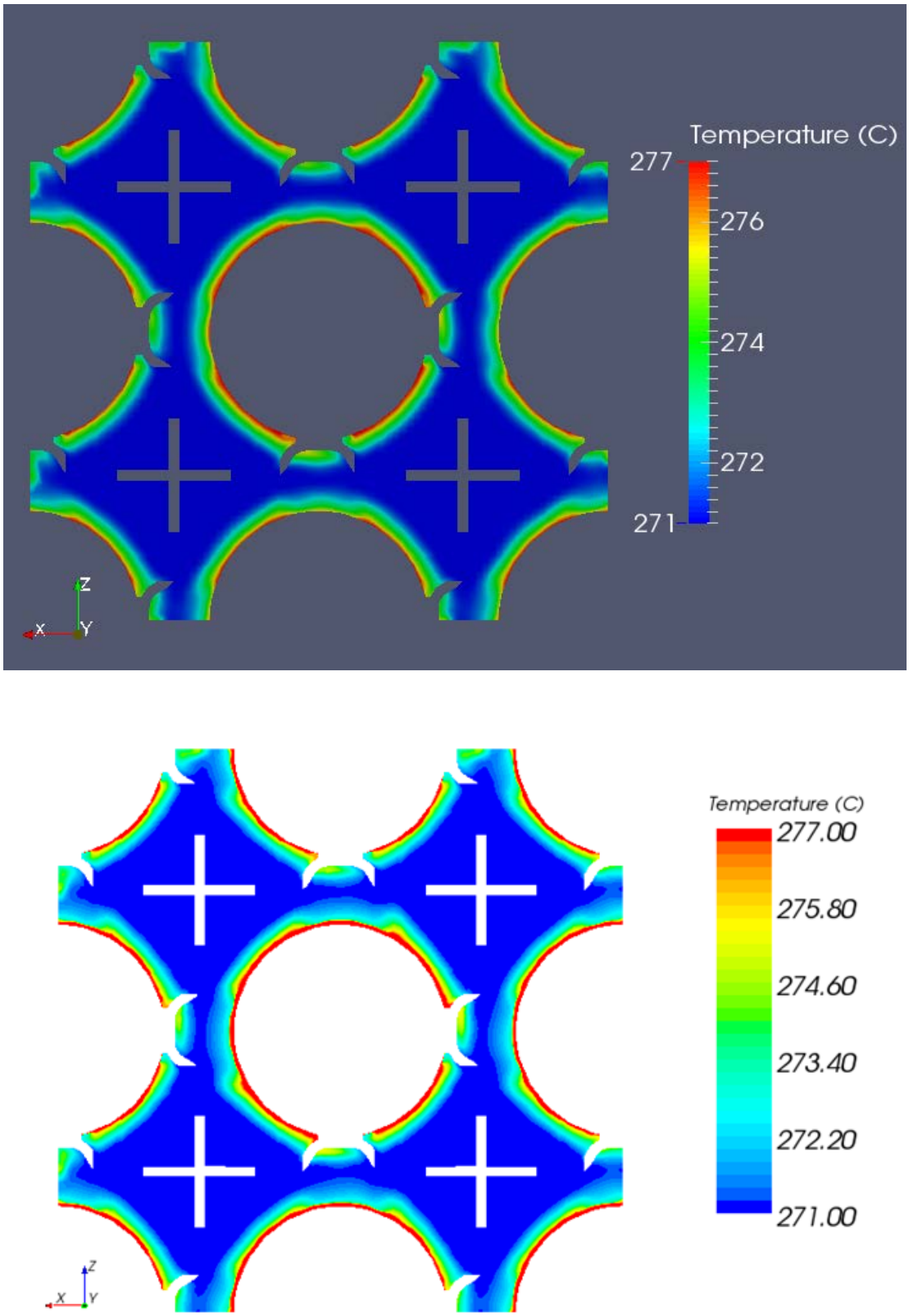

Figure 4.6-5: Temperature contours on horizontal cut plane at Y= - 0.019 m for Hydra-TH (top) and STAR-CCM+ (bottom)

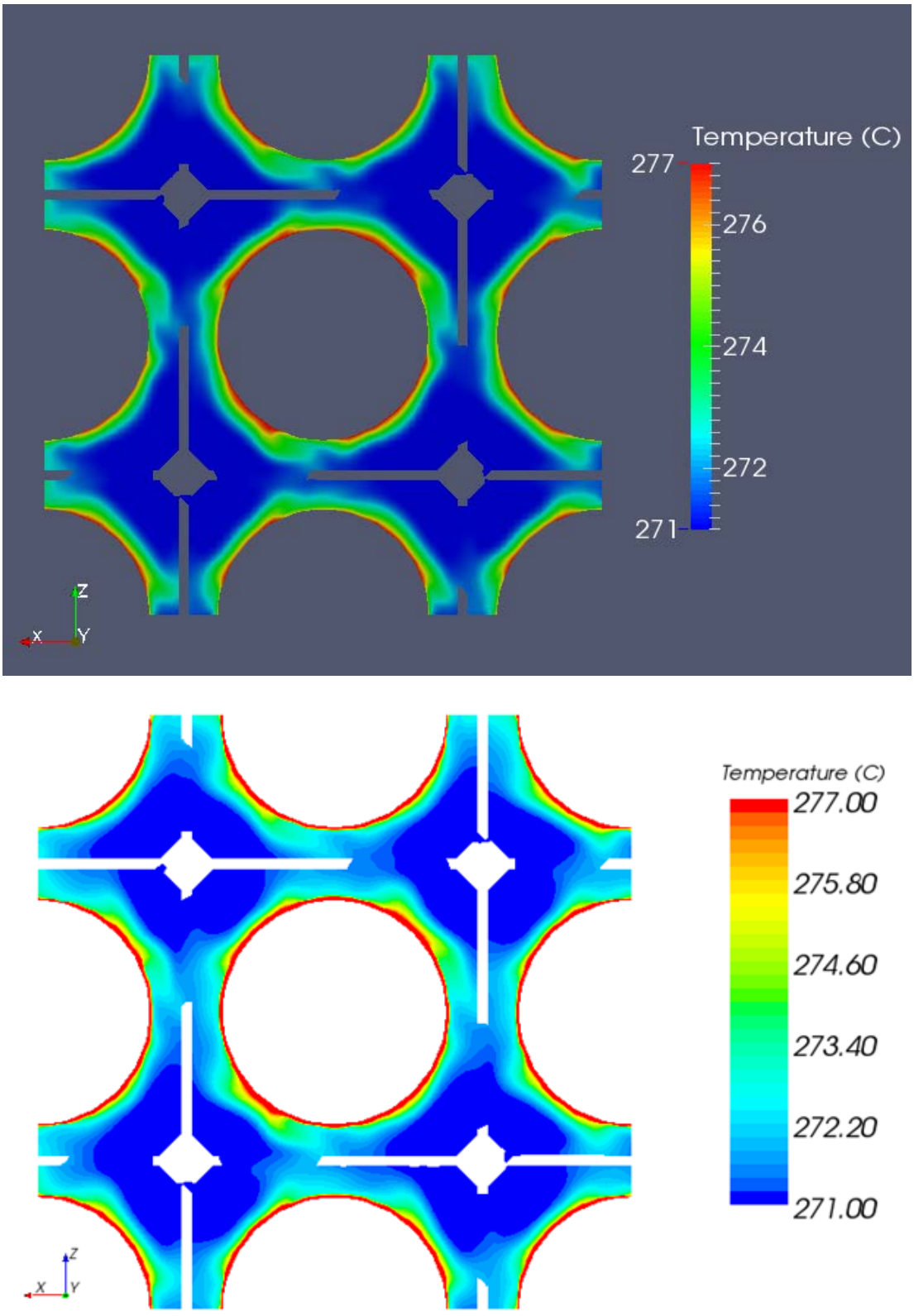

Figure 4.6-6: Temperature contours on horizontal cut plane at Y= 0 m for Hydra-TH (top) and STAR-CCM+ (bottom)

(again note the mesh jumps across the grid surfaces)

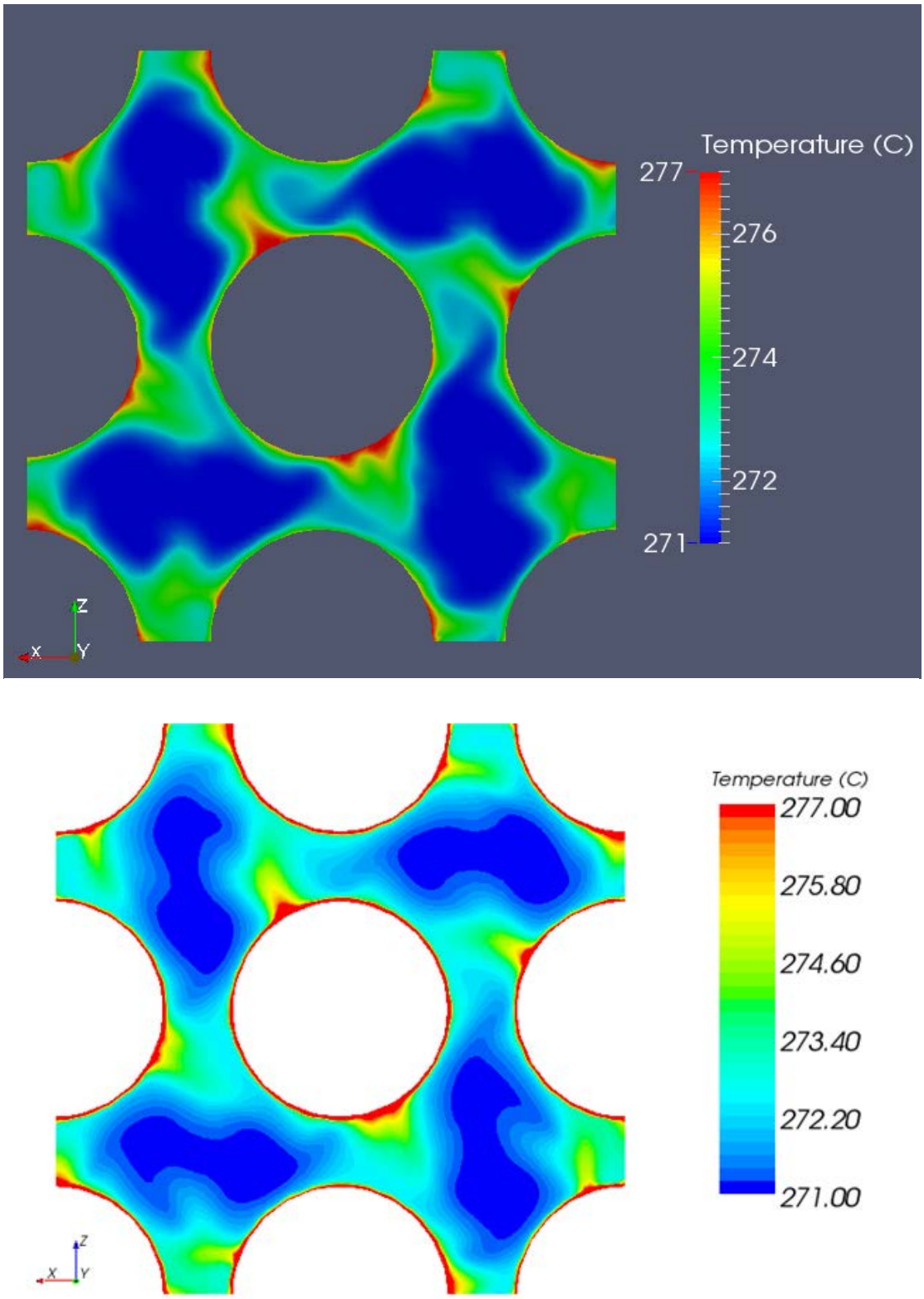

Figure 4.6-7: Temperature contours on horizontal cut plane at Y= 0.017 m for Hydra-TH (top) and STAR-CCM+ (bottom)

4.7 Summary

The Hydra-TH code assessment is summarized below.

- Hexpress/Hybrid, Hydra-TH and ParaView software were all installed, debugged and successfully tested on Westinghouse computer system, **binford**. It is important to note that there was considerable group efforts and support from many partners including LANL [Hydra-TH], Kitware [ParaView] and NUMECA [HEXPRESS/Hybrid] over five months in installing these software on the Westinghouse system and debugging them for use. As of writing this report, all codes are properly functional for the 3x3 modeling and simulation, although additional improvements are needed for modeling larger models such as the 5x5 rod bundle.
- Hexpress/Hybrid version 3.1_1 was installed on the Westinghouse computer system. Some of the code bugs from version 2.12 were cleaned in this version. There are still bugs within the code and these are being communicated to NUMECA as they are discovered (such as such as jumping over features that are clearly captured elsewhere in the same mesh).
- Hexpress/Hybrid mesh for 3x3 single span sub-channel model has been generated for both STAR-CCM+ (.msh) and Hydra-TH (.h5).
- Hydra-TH code was run with the 3x3 single span sub-channel model and post-processed with ParaView. Hydra-TH bugs are being communicated to LANL as they are discovered.

Note: Hexpress/Hybrid, Hydra-TH and ParaView are all new codes being introduced to Westinghouse, and Hydra-TH especially to industry. Thus, successful applications of the Hydra-TH code system require significant efforts of learning by an industrial user and support from the code developers and software vendors, especially when possible deficiencies/bugs of the code(s) are discovered when applied to real world problems. However, the effort for this milestone work and the experience gained through these challenges are already paying back on CASL-related projects such as the DNB CP and the reactor vessel modeling. The script based nature of Hexpress/Hybrid and Hydra-TH is very helpful for the CFD users with regards to experience transfer.

5. TESTING OF GRID HEAT TRANSFER MODEL

In addition to the DNB-related modeling and simulations in the previous sections, additional testing was performed with the Yao-Hochreiter-Leech grid heat transfer model (Reference 11) recently installed in the CTF code (PHI Kanban #3204). Results of the testing show that the model associated user inputs prevented the user from simulating an input model with more than 20 subchannels. In addition, user inputs associated with the grid spacer flow resistance and heat transfer models were identified to need significant improvements for reasonable scope of the simulation application. Discussions have been held between the CTF development and evaluation teams to identify expected areas of error corrections and code improvements relating to the grid spacer models.

6. CONCLUSION AND RECOMMENDATIONS

Significant improvements have been achieved on the CASL multi-scale T/H code and modeling capabilities based on the CTF subchannel code and the Hydra-TH CFD code in the past year for DNB CP applications. The improvements are reflected in the new transient modeling for the RIA DNB predictions and full assembly modeling using the CTF code and its processor, as well as the rod bundle modeling for single-phase flow and heat transfer simulations using the Hydra-TH code, the pre-processor for mesh generation and the post-processor for data visualization. The following code capabilities have been demonstrated in the assessment:

- The modeling and simulation of the TK experiments demonstrated that CTF is able to simulate a fast transient with a large power pulse.

- The CTF preprocessor was found to be very helpful in greatly reducing the model creation effort and minimizing human error for large model setup such as a subchannel model for the entire 17x17 fuel assembly. A reasonably fast CTF execution time can be achieved with the Krylov solver with the large model.

- The modeling and simulation of the 3x3 subchannel geometry under single phase flow conditions have been successfully completed using the Hydra-TH CFD code including mesh generation and result visualization. The Hydra-TH results indicate the similar capabilities of the subchannel single phase fluid solutions as compared to the STAR-CCM+ results.

The code and model assessments also indicated additional improvements needed for the planned DNB CP applications. Recommendations on code specific improvements are listed in the following sections.

6.1 Issues and Suggested Improvements for CTF and Its Preprocessor

During the development of models and the analyses performed for the TK tests in Section 2 and the full assembly model in Section 3, several issues and potential improvements were identified and communicated to the CASL development team. They are now tracked in the PHI Kanban system. A summary list is provided here for completeness:

- The mass storage term as convergence criterion: It would be useful to have a term that actually represents the mass storage through the system, by calculating separately for each phase instead of combing them into an overall storage. This way the phase mass storage can be calculated as positive or negative and works properly for both transient and steady state runs. The mass balance should include the total of the mass storage terms for transient unstable periods. In steady state, the total sum of the mass storage term will be close to zero anyway, so the adding of this mass storage term would not impact the balance results.

- Formatting error in *deck.out*: In the channel output file, flow regime is printed as ";" instead of "11" in the bundle average results table. It is correctly printed in the individual channel tables.

- Formatting in *dnb.out* : It would be useful to limit the DNBR to a relatively low value (e.g., 1000) to eliminate the printout of the DNBR values as "*****".

- Modeling capability outside the active fuel zone: Both the preprocessor and the CTF code need to be updated to include the unheated sections of the fuel rod.

- Pellet radial power profile input: While pellet radial power profile can be defined in CTF for each fuel type, the preprocessor does not have this capability. As such, the CTF inputs created by the preprocessor assume uniform radial power profiles in the pellet.

- Fuel pellet density is not properly passed from the preprocessor to the CTF input deck.

- Initial oxidation input capability in the preprocessor would be a useful option to pass to CTF input deck.

- Channel specific grid loss coefficient: The preprocessor allows a loss coefficient defined only at an axial location and applies that loss coefficient uniformly to every channel at that axial location. CTF has the capability to define different loss coefficients for different channels at an axial location. It is desirable to have the same capability in the preprocessor.

- Restart from a converged steady-state solution using the *restart.in.crs* dump file is currently not working due to array allocation issues.

- Visualization capability for transient behavior and fuel rod temperatures: 3D plotting capabilities need to be expanded to include fuel rod data, such as surface heat flux, pellet and clad temperatures.

- Additional improvements needed for the grid heat transfer modeling option in the CTF code, including the input allowance for more channels and treatment of grid spacer loss coefficients and the heat transfer model.

CTF performance: It would be beneficial to implement additional parallel processing capability within a single assembly to further speed-up the calculations.

6.2 Issues and Suggested Improvements for Hydra-TH and Its Preprocessor

During the development of models and the analyses performed, several issues and potential improvements were identified and communicated to the software developers. A summary list is provided here for completeness:

Hexpress/Hybrid:

- The mesher unexpectedly jumps over CAD features where the same features were captured elsewhere in the model (such as dimple walls of the grids). For large models, it is almost impossible to check every small detail of the mesh to make sure that this did not happen. The mesher should indicate this in the output, or even halt meshing process with a note to refine/update the meshing script/parameters.

- The mesher sometimes gets stuck in refinement loops and this should be communicated in the screen output as a warning during the process (ex: mesher in Nth cycle of refinement, might consider updating script/parameters).

- With some CAD formats, the geometry is imported as for example in milimeters dimensions, but the mesh is generated in meters dimensions.

- Related to above, scaling of geometry in the conf script should be available.

- Better user manuals would definitely be useful. There are features in Hexpress/Hybrid that are not being used due to poor/insufficient documentation and thus user understanding (as example, although a larger and different purpose software, STAR-CCM+ has a user's manual with more than 13,000 pages). Example uses of advanced features are suggested to be documented.

- A full time technical support person with access to export controlled materials is suggested. Lack of this clearance prevents Westinghouse from sharing models with technical support and the communications are then kept generic.

Hydra-TH:

- A more streamlined installation procedure is recommended to open the doors for more industry users. It took considerable effort of expert Westinghouse IS team to get the code running on Westinghouse systems (with tremendous help from LANL). In addition, a CASL dedicated machine with full control was purchased, and if this wasn't an option, it would have been impossible to have Hydra-TH running on Westinghouse systems with various controls/restrictions in place (with regards to pack updates, etc.).

- The core development team for Hydra-TH is thinning out, and if this code is to be used for industry applications, more features may need to be added (such as fully implicit solver) and this requires manpower. Bugs are already being discovered, and the resolution for these may mean more support.

- Fully implicit solver development and implementation is strongly suggested.

ParaView:

- A more streamlined installation procedure is suggested for the developers. The installation of ParaView and using it in parallel on Westinghouse systems took considerable time even with the expertise of the Westinghouse IS team. The delay in functionality of ParaView also delays the post-processing of Hydra-TH results, and slowing down the debugging/learning.

- The 3x3 model presented herein is significantly smaller than the main focuses of the milestones (5x5 rod bundle and eventually quarter and full fuel assembly modeling). But ParaView is using significant resources even with this small model, and responding much slower than expected. Significantly slow (if not crash/freeze) are expected when the 5x5 model loading is attempted.

Testing Hydra-TH and ParaView on larger models (5x5 rod bundle and beyond) is in progress. New feedbacks and additional recommendations during the model development will continue to be communicated to the software and method development team.

7. REFERENCES

1. CASL-I_2013-0110-001, “Challenge Problem Charter: DNB Challenge Problem,” August 2013.

2. CASL-X-2014-0010-000, “DNB CP Implementation Plan,” February 2014.

3. R. Salko, R. Schmidt, R. Hooper, and M. Avramova, “Initial Cobra-TF Parallelization, Milestone Report L3:VRI.PSS.P7.05,” CASL-I-2013-0180-000, August 2013.

4. M. Christon, J. Bakosi and R. Lowrie, "Hydra-TH User's Manual, Version: LA-CC-11120," Tech. report LA-UR-12-23181, LANL, 2011.

5. Fuketa, T., et al., “NSRR/RIA Experiments with High-Burnup PWR Fuels,” *Nuclear Safety*, Vol.37, No. 4, Nuclear Regulatory Commission, Bethesda, Maryland, October-December, 1996, pp.328-342.

6. “Analysis of Reactivity Initiated Accident-Simulation Tests Conducted at the CABRI and NSRR Facilities in France and Japan” EPRI Technical Report, 1002863**,** 2003**.**

7. Salko, R. K and M. Avramova, “CTF Pre-processor User's Manual,” The Pennsylvania State University, November 21, 2013.

8. Salko, R. K and M. Avramova, “CTF Theory Manual,” The Pennsylvania State University, May 1, 2013.

9. Sung, Y. et al., “Evaluation and Application of Updated VERA T/H Codes for DNB-Related Data Analysis” L3.AMA.CHLNG.P7.02, September 2013.

10. WCAP-15306-NP-A, “VIPRE-01 Modeling and Qualification for Pressurized Water Reactor Non-LOCA Thermal-Hydraulic Safety Analysis,” Westinghouse, October 1999.

11. Yao, S.C., et al., “Heat Transfer Augmentation in Rod Bundles Near Grid Spacers,” ASME 80-WA/HT-62, 1980.

12. LANL Hydra-TH (https://get-hydra.lanl.gov/)

13. CD-adapco STAR-CCM+ (http://www.cd-adapco.com/products/star-ccm%C2%AE)

14. Dassault Systèmes SolidWorks (http://www.solidworks.com/default.htm)

15. NUMECA Hexpress/Hybrid (http://www.numeca.com/en/products/automeshtm/hexpresstmhybrid)

16. Kitware ParaView (www.paraview.org/)

17. MT-13-40, “Transmittal of Proprietary DNB Data and Information to CASL,” Westinghouse, March 2013.